

Notice

This project was funded by the Department of Transportation, Pipeline and Hazardous Materials Safety Administration under the Pipeline Safety Research and Development Program. The views and conclusions contained in this document are those of the authors and should not be interpreted as representing the official policies, either expressed or implied, of the Pipeline and Hazardous Materials Safety Administration, or the U.S. Government.



Natural Resources
Canada

Ressources naturelles
Canada

Disclaimer

Natural Resources Canada makes no representations or warranties respecting the contents of this report, either expressed or implied, arising by law or otherwise, including but not limited to implied warranties or conditions of merchantability or fitness for a particular purpose.



Natural Resources
Canada

Ressources naturelles
Canada

Acknowledgements

Thanks are due to several technical staff members at CanmetMATERIALS, including Mr. J. Liang for performing mechanical testing, Ms. P. Liu and Ms. R. Zavadil for metallographic analysis and microhardness testing as well as Mr. J-P. Talon and Mr. D. Sebesta for their machining expertise. The support and guidance provided by Dr. M. Arafin, Program Manager-Pipelines is also appreciated. Additional funding provided by the Federal Program for Energy Research and Development (PERD) and Natural Resources Canada greatly acknowledged.



Natural Resources
Canada

Ressources naturelles
Canada

Table of Contents

Notice	i
Disclaimer	ii
Acknowledgements	iii
Nomenclature	A-1
Abbreviations	A-1
Organizations	A-1
Appendix A Properties of Materials Used for Full-Scale Tests	A-2
A.1 Tensile Testing of Selected Pipes	A-2
A.2 Tensile Property Data for Selected Steel Pipes	A-3
A.3 Compression Testing of Selected pipes	A-14
A.4 Compression and Tension Properties of Selected Pipes Used for Full-Scale Tests	A-14
A.5 Chemical Analysis, Metallography and Microhardness Testing of Selected Pipes	A-19
A.6 Chemical Compositions, Microstructure and Microhardness of Selected Pipes	A-19
A.7 References	A-36

Nomenclature

Abbreviations

BL	Bondline
CGHAZ	Coarse grain HAZ
DSAW	Double submerged arc welding
EL	Elongation
ERW	Electric resistance welding
HAZ	Heat affected zone
ICR	Intercritically Reheated
ID	Inside diameter
LPA	Longitudinal-to-pipe axis
OD	Outside diameter
PWHT	Post weld heat treatment
TPA	Transverse-to-pipe axis
uEL	Uniform strain (uniform elongation)
UTS	Ultimate tensile strength
VHN	Vicker hardness Number
WM	Weld metal
WMC	Weld metal centerline
WT	Wall thickness
Y/T	Yield to tensile strength ratio

Organizations

CRES	Center for Reliable Energy Systems,
PHMSA	Pipeline and Hazardous Materials Safety Administration,

Appendix A Properties of Materials Used for Full-Scale Tests

This Appendix summarizes the testing and evaluation of the small diameter steel pipe materials that were used for the full-scale tests carried out in this project. The data and results were used to verify actual pipe material properties by use of tensile and compression testing as well as limited optical microscopy and microhardness assessments that would help with understanding the consistency and/or variations in measured properties.

A.1 Tensile Testing of Selected Pipes

Duplicate sub-size strip tensile and full-thickness strap tensile specimens were cut and machined from selected X65/X70 ERW pipes and an X80 DSAW pipe, in order to characterize the pipe steel properties in more detail. The pipes and their nominal dimensions are listed below.

- X65 ERW-1(a), 1(b), 1(c) pipe sections: 324 mm OD x 6.35 mm W.T. (12.75" x 0.250")
- X65 ERW-2 pipe sections: 324 mm OD x 9.52 mm W.T. (12.75" x 0.375")
- X70 ERW-3 pipe sections: 324 mm OD x 7.14 mm W.T. (12.75" x 0.281")
- X80 DSAW pipe sections: 610 mm OD x 12.7 mm W.T. (24.0" x 0.500")

Both transverse and longitudinal specimens were cut from close to the 3:00 or 9:00 and 6:00 clock positions, as shown in the schematic diagrams in Figure A1. The small-strip specimens were machined in the transverse-to-pipe-axis (TPA) direction with the maximum possible thickness used for the small diameter pipes and their respective wall thicknesses. The full-thickness strap tensile specimens were waterjet profiled with a longitudinal-to-pipe-axis (LPA) orientation from the same clock positions. Table A1 provides the details of the gauge dimensions for the TPA and LPA tensile specimens, while drawings of the individual TPA tensile specimens and a typical example of the LPA specimens are presented in Figures A2 and A3, respectively.

All testing was performed using a hydraulic universal testing machine with the required capacity and appropriate sized wedge grips for the TPA and LPA specimens. In the former case, the small specimens had gauge length (25.4 mm) marks scribed on reduced section where an extensometer was also positioned to record the displacement and provide a measure of strain. Much longer (~285 mm) full-thickness strap tensile specimens were waterjet cut with an overall reduced section of 101.6 mm. Three separate pairs of gauge marks (50.8 mm spacing) were marked along the full reduced section to ensure the point of fracture was within a given pair of marks. The 50.8 mm wide extensometer was centered on the reduced section. All tensile testing was performed at room temperature following general guidelines provided in ASTM E8M. The reported tensile property data includes 0.2% offset and 0.5% underload yield strengths, ultimate tensile strength (UTS), Y/T ratios, uniform strain, and total elongations (measured by the extensometer and by gauge marks after testing). Stress vs strain curves were created to allow comparisons of selected tests for the different orientations (TPA and LPA) and clock positions.

A.2 Tensile Property Data for Selected Steel Pipes

Tables A2 and A3 provide the complete list of tensile property results obtained for the duplicate tests conducted to assess two different orientations and two clock positions. These data show that the results from the duplicate tests were generally very consistent, while there were some differences in tensile properties observed as function of test specimen orientation and clock position, which is further evident in the average results provided in Tables A4 and A5. Specific examples of the tensile properties obtained for the selected pipe steels are presented in the series of Tables A6 to A9 and graphically in corresponding stress-strain curves in Figures A4 to A8.

For the three X65 ERW-1 steel pipe sections the results were very consistent and repeatable and followed the same overall trends. The results showed an unexpectedly large difference in yield strengths and post yielding behavior as a function of clock position for both TPA and LPA specimen orientations (Table A6 and Figure A4). Along with the higher yield strengths for the 6:00 position, both the UTS and Y/T values were marginally higher, while the uniform strains and total elongations were considerably lower than those for the 3:00 specimens.

The X65 ERW-2 pipe steel exhibited tensile properties that were very similar as a function clock position (3:00 and 6:00) for the respective specimen orientation, i.e., TPA or LPA (Table A7 and Figure A5). The specimens from the LPA orientation exhibited marginally higher yield strengths and Y/T ratios in conjunction with lower uniform strain and total elongation values.

The tensile property results for the X70 ERW-3 pipe steel presented in Table A8 and Figure A6, show relative consistent trends with respect to specimen orientation and clock position. In this case, the yield strengths were marginally higher for the LPA specimens, while the UTS values were lower compared with the TPA specimens. This resulted in slightly higher Y/T ratios, with similar uniform strains and total elongation values.

Table A9 lists the tensile properties obtained for the X80-DSAW pipe steel, while Figure A7 shows the corresponding stress-strain curves as a function of specimen orientation and clock position. Although the results show that the specimens from 6:00 exhibited slightly higher yield strengths, UTS, and Y/T values, the major differences beyond the peak stress were dominated by specimen orientation (TPA vs LPA). In this case, larger values for uniform strain and total elongation were observed for the TPA specimen orientation.

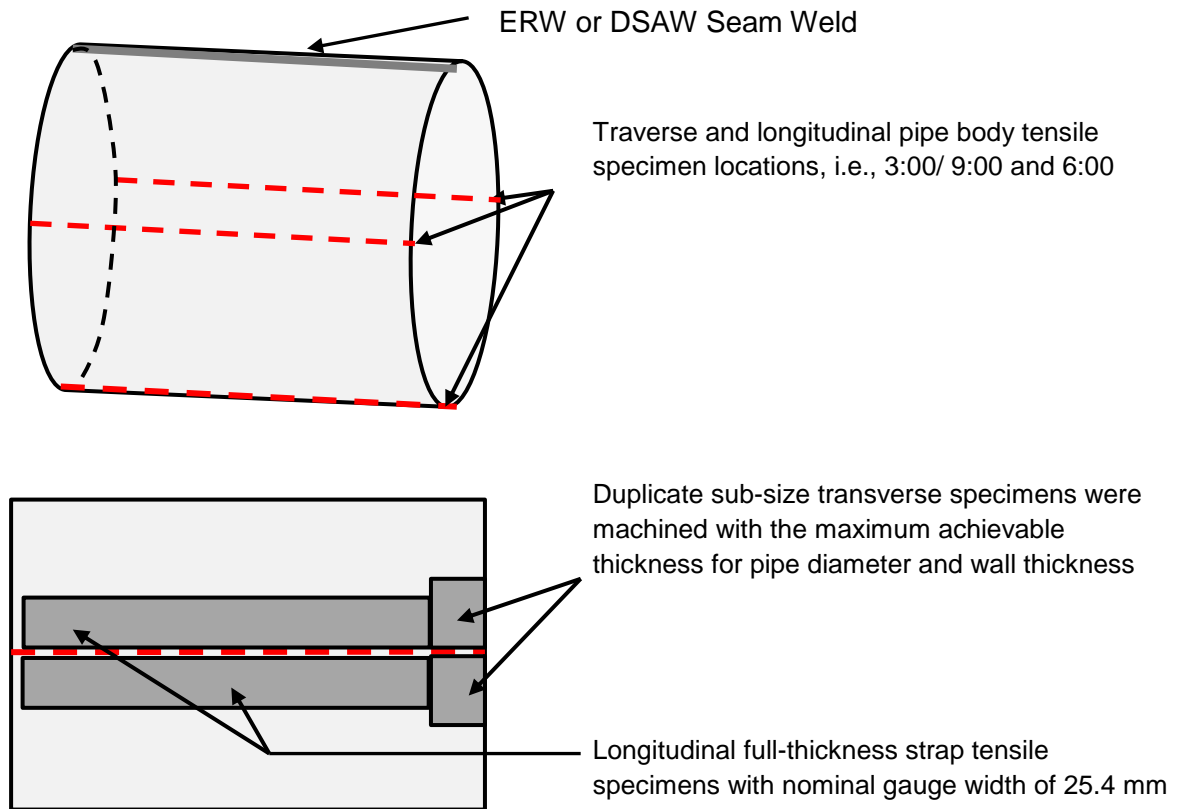
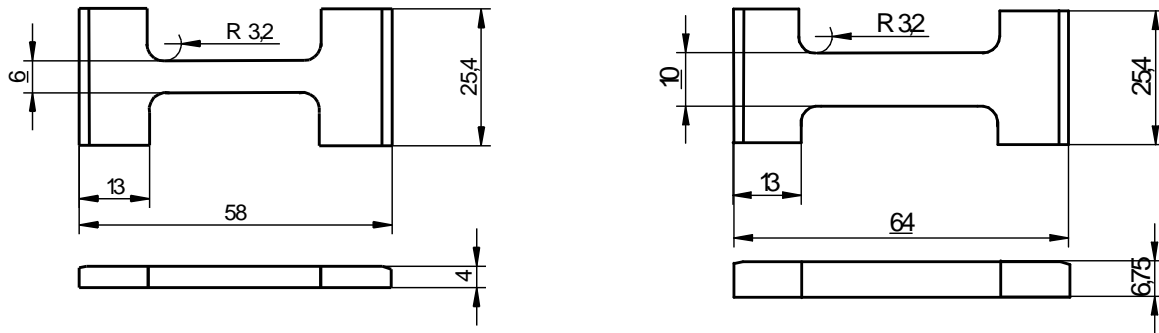


Figure A1 Schematic diagrams showing location and orientation of pipe body tensile specimens from ERW and DSAW pipes

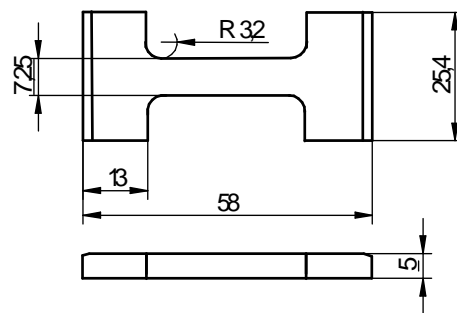
Table A1 Detail of Pipes and Corresponding Tensile Specimens

Pipe ID	Pipe Diameter and Wall Thickness mm	Specimens Gauge Section Dimensions Width x Thickness mm	
		TPA	LPA
ERW-1(a), 1(b), and 1(c)	324 mm OD x 6.35 mm W.T.	6 x 4	25.4 x 6.4
ERW-2	324 mm OD x 9.52 mm W.T.	10 x 6.7	25.4 x 9.5
ERW-3	324 mm OD x 7.14 mm W.T.	7.25 x 5	25.4 x 7.25
X80-DSAW	610 mm OD x 12.7 mm W.T.	14.1 x 9.5	25.4 x 12.7

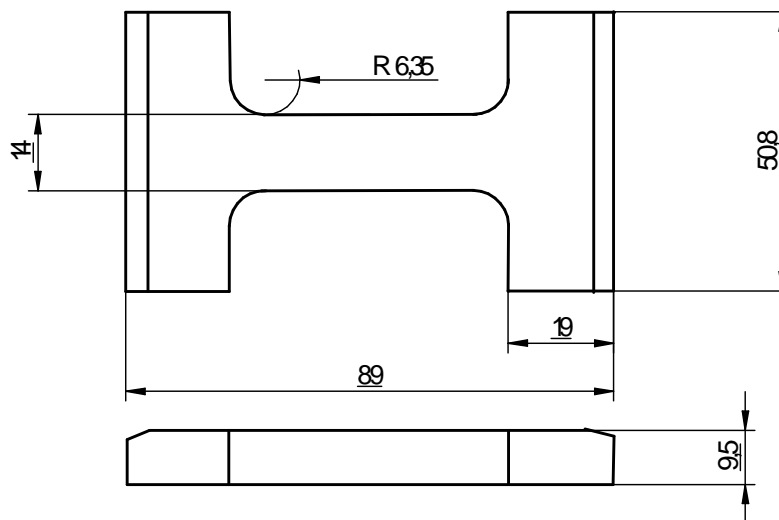


(a) X65 ERW-1

(b) X65 ERW-2



(c) X70 ERW-3



(d) X80 DSAW

Figure A2 Drawings showing the geometry and dimensions of TPA pipe steel tensile specimens

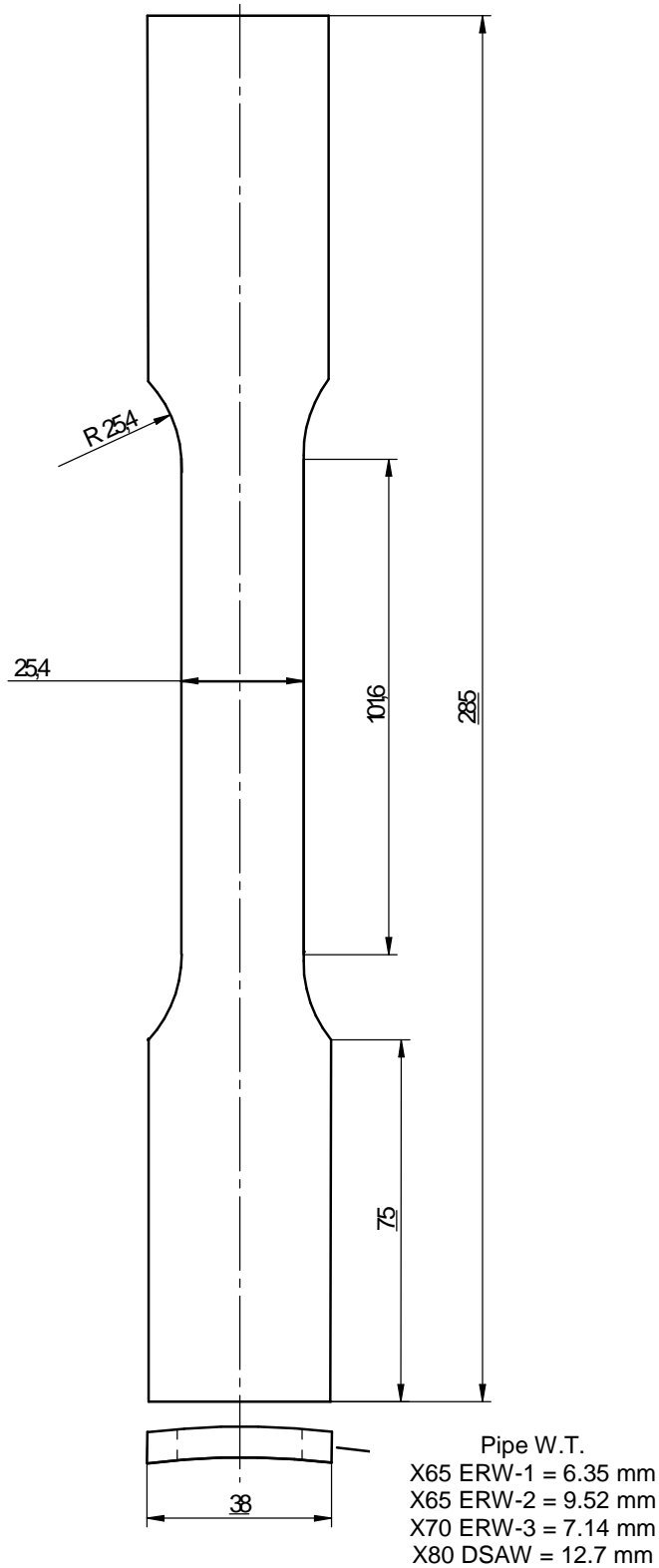


Figure A3 Representative drawing showing the geometry of the full-thickness LPA tensile specimen. Note the different W.T. of individual ERW pipes.

Table A2 List of Tensile properties for X65 ERW pipes

Pipe ID	Specimen Orientation	Specimen ID	Yield 0.2% (MPa)	Yield 0.5% (MPa)	UTS (MPa)	0.2% Y/T	0.5% Y/T	uEL (%)	EL- 1 (%)	EL- 2 (%)	
X65 ERW-1(a)	TPA	3:00-A	460	470	563	0.82	0.83	13.4	30	32	
		3:00-B	442	454	561	0.79	0.81	13.2	29	30	
		6:00-A	496	509	578	0.86	0.88	5.1	24	25	
		6:00-B	510	523	581	0.88	0.90	6.8	23	24	
	LPA	3:00-A	NA	NA	NA	NA	NA	NA	NA	NA	NA
		3:00-B	474	481	537	0.88	0.90	13.2	33	34	
		6:00-A	550	554	565	0.97	0.98	4.5	28	30	
		6:00-B	550	552	560	0.98	0.99	2.6	27	28	
X65 ERW-1(b)	TPA	3:00-A	448	460	554	0.81	0.83	16	31	31	
		3:00-B	493	449	551	0.89	0.81	14.1	29	30	
		6:00-A	489	504	573	0.85	0.88	8.2	23	25	
		6:00-B	498	509	579	0.86	0.88	9.5	26	27	
	LPA	3:00-A	471	471	528	0.89	0.89	15.9	35	36	
		3:00-B	453	456	520	0.87	0.88	16	35	35	
		6:00-A	535	538	551	0.97	0.98	6.3	30	31	
		6:00-B	526	529	546	0.96	0.97	8.3	29	29	
X65 ERW-1(c)	TPA	3:00-A	445	461	551	0.81	0.84	13.3	30	31	
		3:00-B	430	448	554	0.78	0.81	13.2	29	30	
		6:00-A	498	512	577	0.86	0.89	8.7	23	23	
		6:00-B	500	514	582	0.86	0.88	6.6	24	25	
	LPA	3:00-A	466	469	527	0.88	0.89	14.4	34	35	
		3:00-B	458	461	525	0.87	0.88	13.9	34	35	
		6:00-A	543	545	559	0.97	0.97	3.4	26	27	
		6:00-B	547	549	563	0.97	0.98	4.7	31	31	
X65 ERW-2	TPA	3:00-A	432	442	539	0.80	0.82	11.2	38	40	
		3:00-B	424	436	531	0.80	0.82	11.9	39	41	
		6:00-A	440	450	526	0.84	0.86	11.3	39	40	
		6:00-B	453	461	535	0.85	0.86	10.2	38	39	
	LPA	3:00-A	473	480	529	0.89	0.91	9.3	33	35	
		3:00-B	465	474	526	0.88	0.90	8.8	36	37	
		6:00-A	490	495	524	0.94	0.94	7.1	33	34	
		6:00-B	491	497	528	0.93	0.94	8.2	35	34	

Notes: TPA= Transverse-to-pipe axis, LPA= Longitudinal-to-pipe axis; EL-1 = Extensometer and EL-2 = Measured

Table A3 List of Tensile properties for X70 ERW and X80 DSAW pipes

Pipe ID	Specimen Orientation	Specimen ID	Yield 0.2% (MPa)	Yield 0.5% (MPa)	UTS (MPa)	0.2% Y/T	0.5% Y/T	uEL (%)	EL- 1 (%)	EL- 2 (%)
X70 ERW-3	TPA	3:00-A	545	553	677	0.81	0.82	10	28	30
		3:00-B	551	558	672	0.82	0.83	10.2	30	31
		6:00-A	548	558	680	0.81	0.82	9.4	23	30
		6:00-B	543	553	674	0.81	0.82	9.1	28	28
	LPA	3:00-A	564	568	632	0.89	0.90	9.2	27	28
		3:00-B	565	568	638	0.89	0.89	10.5	29	31
		6:00-A	579	581	646	0.90	0.90	9.4	27	28
		6:00-B	575	578	644	0.89	0.90	9.3	28	29
X80 DSAW	TPA	3:00-A	645	645	699	0.92	0.92	6	35	40
		3:00-B	650	649	691	0.94	0.94	5.9	32	38
		6:00-A	704	704	716	0.98	0.98	4.6	34	39
		6:00-B	699	698	714	0.98	0.98	3.7	30	36
	LPA	3:00-A	617	613	685	0.90	0.89	3.9	24	28
		3:00-B	615	614	680	0.90	0.90	4.1	26	30
		6:00-A	643	638	693	0.93	0.92	3.3	8.4	28
		6:00-B	641	635	693	0.92	0.92	2.8	24	27

Notes: TPA= Transverse-to-pipe axis, LPA= Longitudinal-to-pipe axis; EL-1 = Extensometer and EL-2 = Measured

Table A4 List of Average Tensile properties for X65 Pipes

Pipe ID	Specimen Orientation	Specimen ID	Yield 0.2% (MPa)	Yield 0.5% (MPa)	UTS (MPa)	0.2% Y/T	0.5% Y/T	uEL (%)	EL- 1 (%)	EL- 2 (%)
X65 ERW-1	TPA	03:00	453	457	556	0.82	0.82	13.9	30	31
		06:00	499	512	578	0.86	0.89	7.5	24	25
	LPA	03:00	464	468	527	0.88	0.89	14.7	34	35
		06:00	542	545	557	0.97	0.98	5.0	29	29
X65 ERW-2	TPA	03:00	428	439	535	0.80	0.82	11.6	39	41
		06:00	447	456	531	0.85	0.86	10.8	39	40
	LPA	03:00	469	477	528	0.89	0.91	9.1	35	36
		06:00	491	496	526	0.94	0.94	7.7	34	34

Table A5 List of Average Tensile properties for X70 and X80 Pipes

Pipe ID	Specimen Orientation	Specimen ID	Yield 0.2% (MPa)	Yield 0.5% (MPa)	UTS (MPa)	0.2% Y/T	0.5% Y/T	uEL (%)	EL- 1 (%)	EL- 2 (%)
X70 ERW-3	TPA	03:00	548	556	675	0.82	0.83	10.1	29	31
		06:00	546	556	677	0.81	0.82	9.3	26	29
	LPA	03:00	565	568	635	0.89	0.90	9.9	28	30
		06:00	577	580	645	0.90	0.90	9.4	28	29
X80 DSAW	TPA	03:00	648	647	695	0.93	0.93	6.0	34	39
		06:00	702	701	715	0.98	0.98	4.2	32	38
	LPA	03:00	616	614	683	0.90	0.90	4.0	25	29
		06:00	642	637	693	0.93	0.92	3.1	16	28

Table A6 Typical Tensile Properties of X65 ERW-1(c) Pipe Body

Specimen Orientation/ Clock Position	Yield 0.2% MPa	Yield 0.5 % MPa	UTS MPa	0.2%Y/T	Uniform Strain %	Elongation %
TPA-3:00	430	448	554	0.78	13.2	29
TPA-6:00	498	512	577	0.86	8.7	23
LPA-3:00	458	461	525	0.87	13.9	34
LPA-6:00	543	545	559	0.97	3.4	26

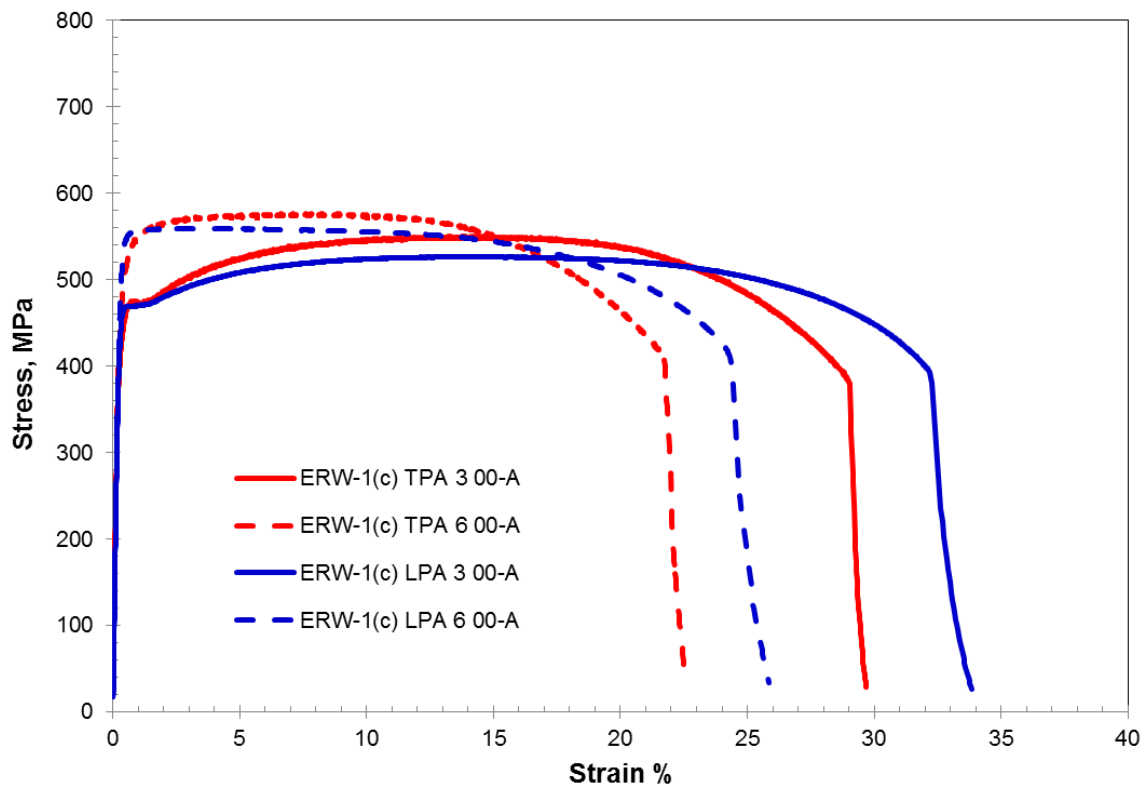


Figure A4 Representative stress-strain curves for X65 ERW-1(c) pipe body as a function of orientation (TPA and LPA) and clock position (3:00 and 6:00)

Table A7 Typical Tensile Properties of X65 ERW-2 Pipe Body

Specimen Orientation/ Clock Position	Yield 0.2% MPa	Yield 0.5 % MPa	UTS MPa	0.2%Y/T	Uniform Strain %	Elongation %
TPA-3:00	432	442	539	0.80	11.2	38
TPA-6:00	440	450	526	0.84	11.3	39
LPA-3:00	473	480	529	0.89	9.3	33
LPA-6:00	490	495	524	0.94	7.1	33

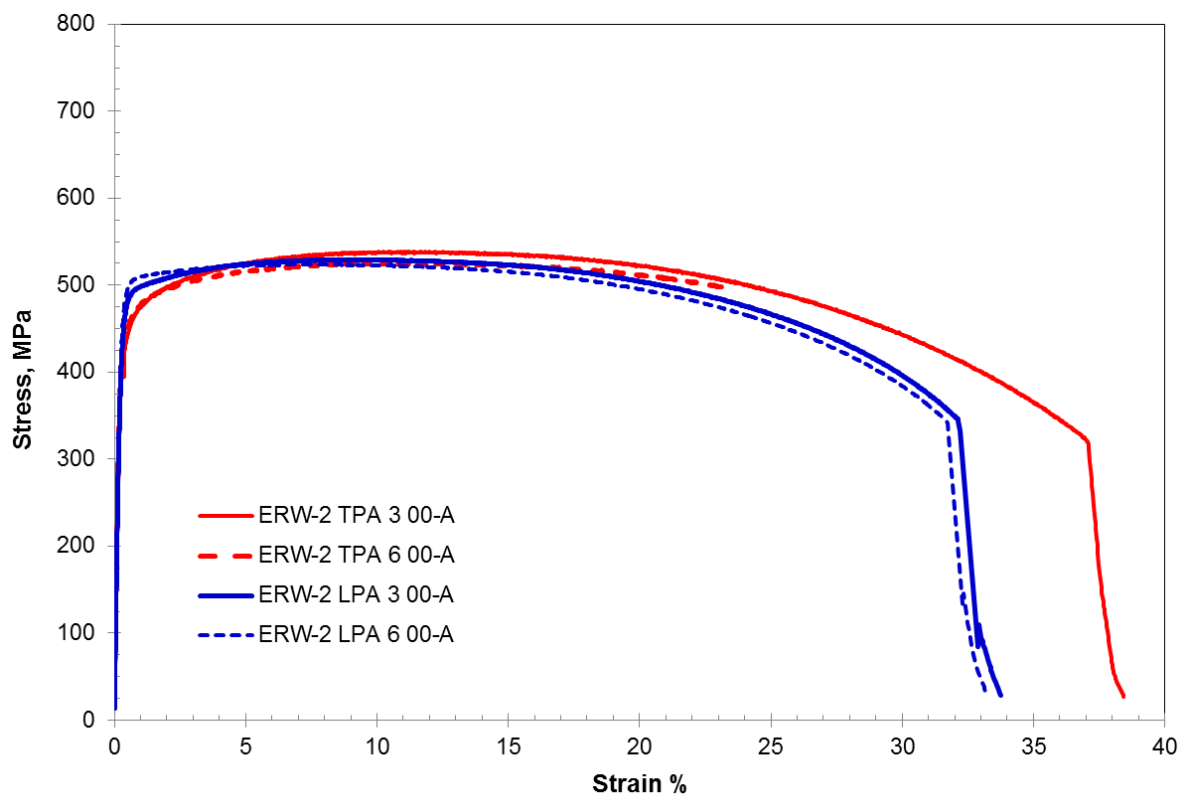


Figure A5 Representative stress-strain curves for X65 ERW-2 pipe body as a function of orientation (TPA and LPA) and clock position (3:00 and 6:00)

Table A8 Typical Tensile Properties of X70 ERW-3 Pipe Body

Specimen Orientation/ Clock Position	Yield 0.2% MPa	Yield 0.5 % MPa	UTS MPa	0.2%Y/T	Uniform Strain %	Elongation %
TPA-3:00	551	558	672	0.82	10.2	30
TPA-6:00	543	553	674	0.81	9.1	28
LPA-3:00	564	568	632	0.89	9.2	27
LPA-6:00	575	578	644	0.89	9.3	28

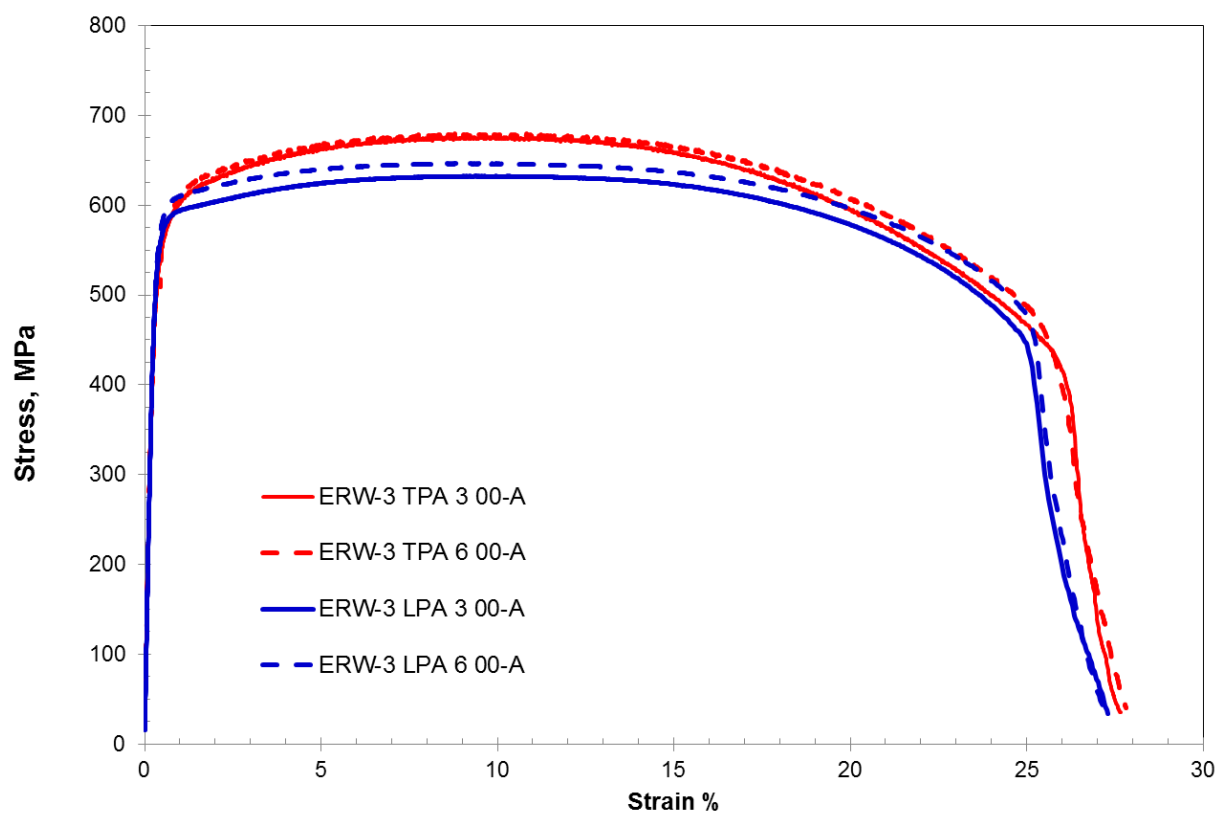


Figure A6 Representative stress-strain curves for X70 ERW-3 pipe body as a function of orientation (TPA and LPA) and clock position (3:00 and 6:00)

Table A9 Typical Tensile Properties of X80 DSAW Pipe Body

Specimen Orientation/ Clock Position	Yield 0.2% MPa	Yield 0.5 % MPa	UTS MPa	0.2%Y/T	Uniform Strain %	Elongation %
TPA-3:00	645	645	699	0.92	6.0	35
TPA-6:00	699	698	714	0.98	3.7	30
LPA-3:00	615	614	680	0.90	4.1	26
LPA-6:00	641	635	693	0.92	2.8	24

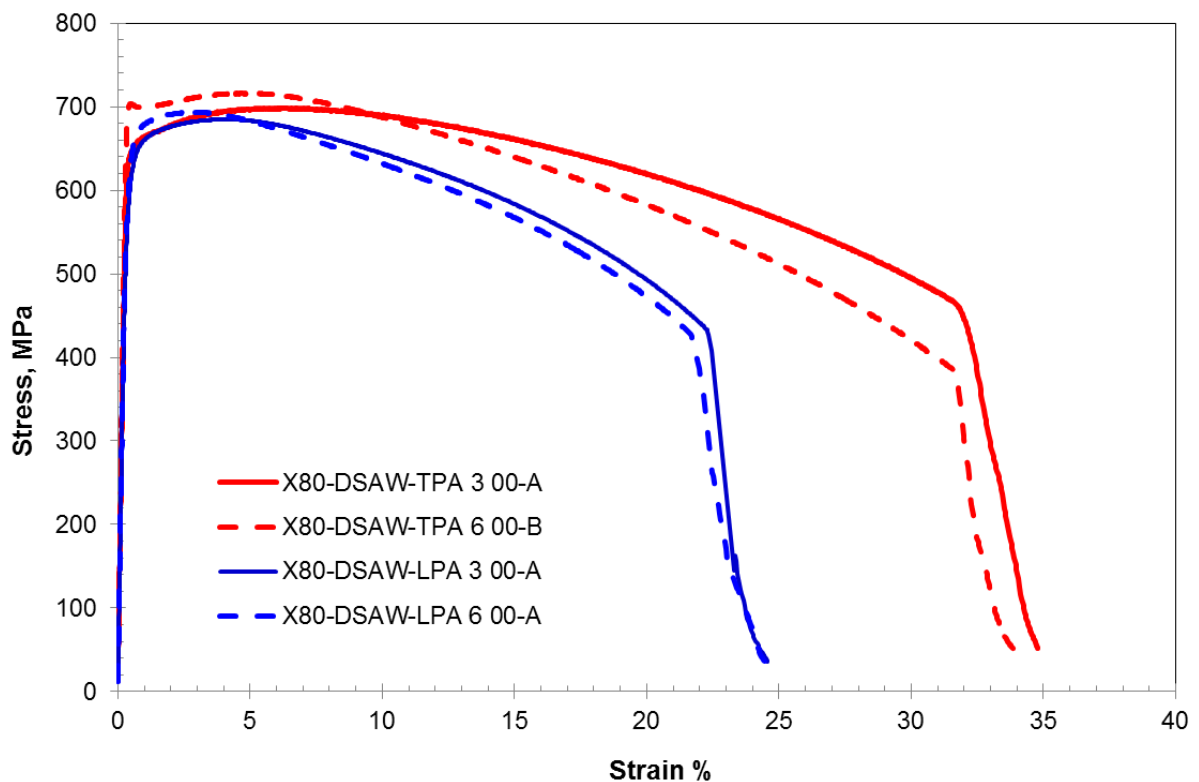


Figure A7 Representative stress-strain curves for ERW-3 pipe body as a function of orientation (TPA and LPA) and clock position (3:00 and 6:00)

A.3 Compression Testing of Selected pipes

Cylindrical specimens with diameters as close to the pipe wall thicknesses as possible were machined from longitudinal to pipe axis (LPA) strips cut from the 3:00 and 6:00 positions of selected ERW and DSAW pipe steels. The specimens were machined to their respective diameters with a constant length to diameter ratio of 3:1 as shown in Figure A8.

Two self-aligning sub-press assemblies were also fabricated to improve the quality of compression testing by reducing the tendency of premature buckling and the effects of friction by use of polished tungsten carbide anvils (Figure A9). The smaller diameter specimens were tested in a 25.4 mm diameter sub-press and required use of non-contact video extensometer to record strain because of their relatively short lengths. For the thicker pipe, X80-DSAW (12.7 mm W.T.) the 12 mm diameter specimens were tested using a 38-mm diameter sub-press with the strain monitored by use of an extensometer set to a gauge length of $2/3L = 24$ mm.

A.4 Compression and Tension Properties of Selected Pipes Used for Full-Scale Tests

The yield strength results obtained for the pipe steels are listed in the series of Tables A10 to A12, while corresponding true stress versus true strain curves are shown in Figures A10 to A12. In general, the compression yield strengths and true stress strain curves were very consistent for a given pipe steel and the respective 3:00 or 6:00 clock positions.

For the X65 ERW-1(c) pipe steel (Table A10), near identical yield strengths were obtained for both compression and tension tests from the 3:00 position. The trend for higher yield strengths obtained for the tension specimens from 6:00 position was also observed for the corresponding compression tests. In this case, the results were slightly lower than for the corresponding tension tests. Figure A10 clearly shows that the compression and tension curves were very close at or just beyond yield, but that the compression curves tended to be marginally higher for larger strains.

The results (Table A11) for the X70 ERW-3 pipe steel were very consistent for both compression and tension tests. The trend of marginally higher yield strength results for the tests from the 6:00 position is evident in the true stress-true strain curves shown in Figure A11.

Very consistent and similar trends for both tension and compression tests were observed for the X80 DSAW pipe steel, as shown in Table A12 and Figure A12. The trend of slightly higher yield strengths for the test specimens from the 6:00 position is also clearly evident.

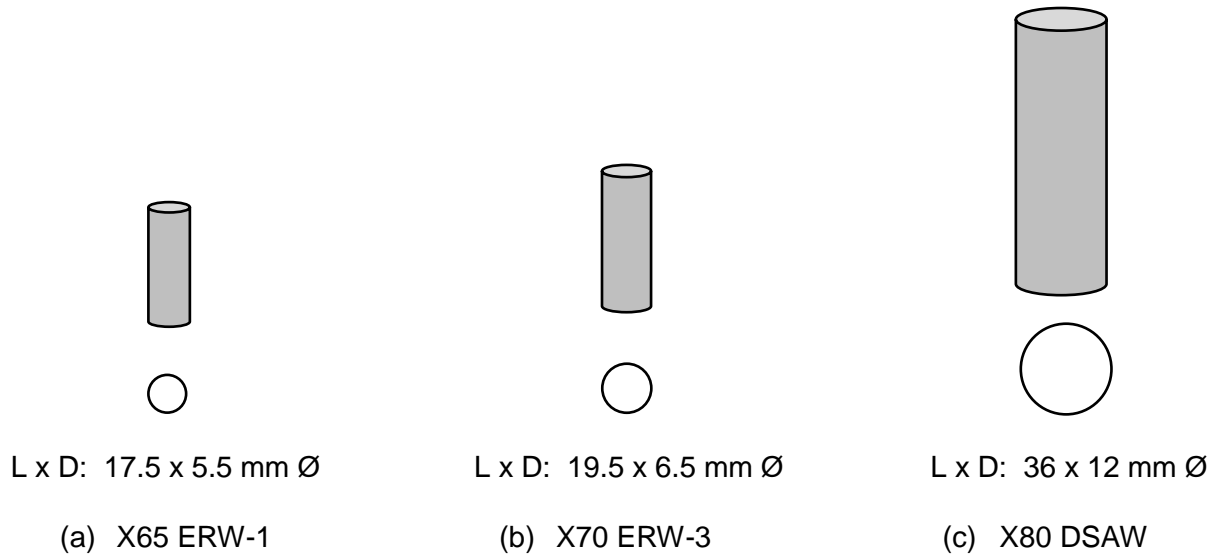


Figure A8 Schematic diagram of compression test specimens with L to D ratio = 3

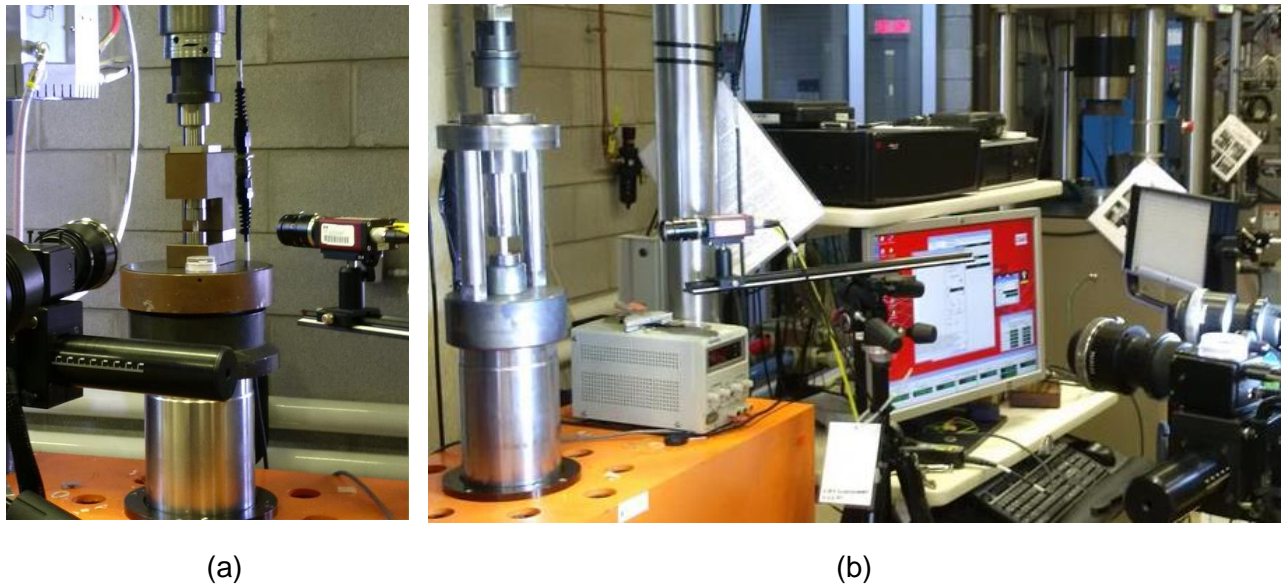


Figure A9 Photographs of test set up for compression testing using (a) small-sub-press and (b) large sub-press for improved alignment and polished tungsten carbide anvil inserts to reduce friction

Table A10 LPA Tensile and Compression Yield Strengths for X65 ERW-1(c) Pipe Body

Pipe Steel	Orientation – Clock Position	Yield Strength, MPa
ERW-1(c)	Tension-3:00	466, 458
	Compression-3:00	460, 460, 464
	Tension-6:00	543, 547
	Compression-6:00	518, 529, 532

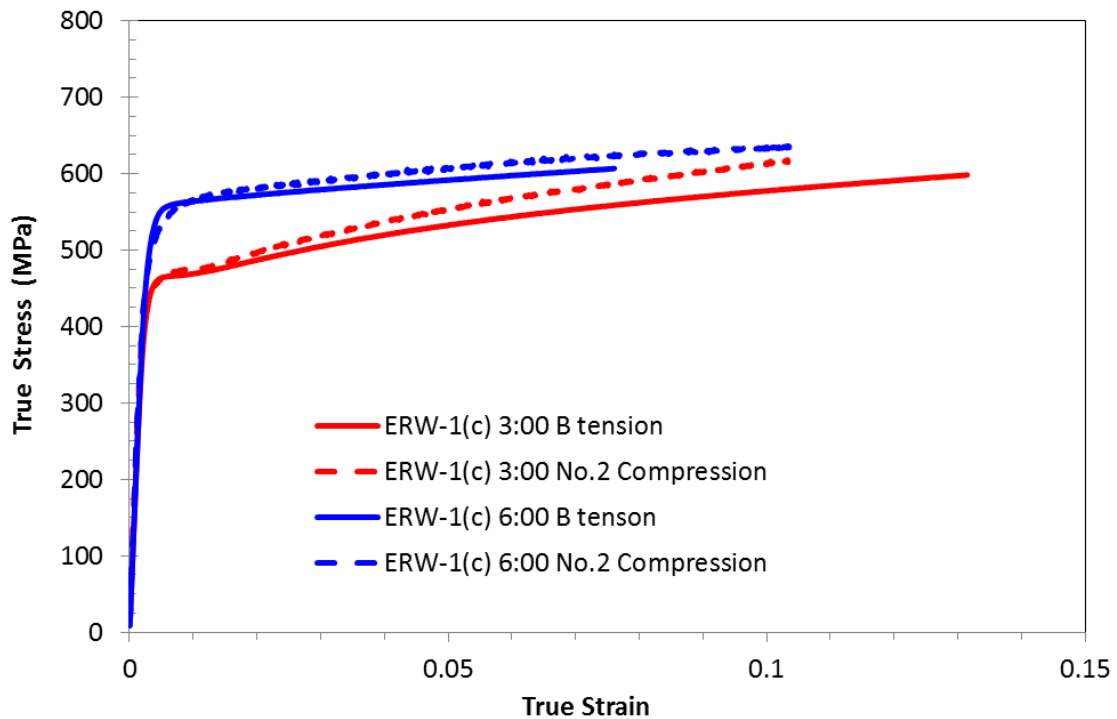


Figure A10 Representative true stress-true strain curves for LPA tension and compression tests for the 3:00 and 6:00 positions of X65 ERW-1(c) pipe steel

Table 11 LPA Tensile and Compression Yield Strengths for X70 ERW Pipe Body

Pipe Steel	Orientation – Clock Position	Yield Strength, MPa
ERW-3	Tension-3:00	564, 565
	Compression-3:00	548, 551
	Tension-6:00	579, 575
	Compression-6:00	564, 558, 576

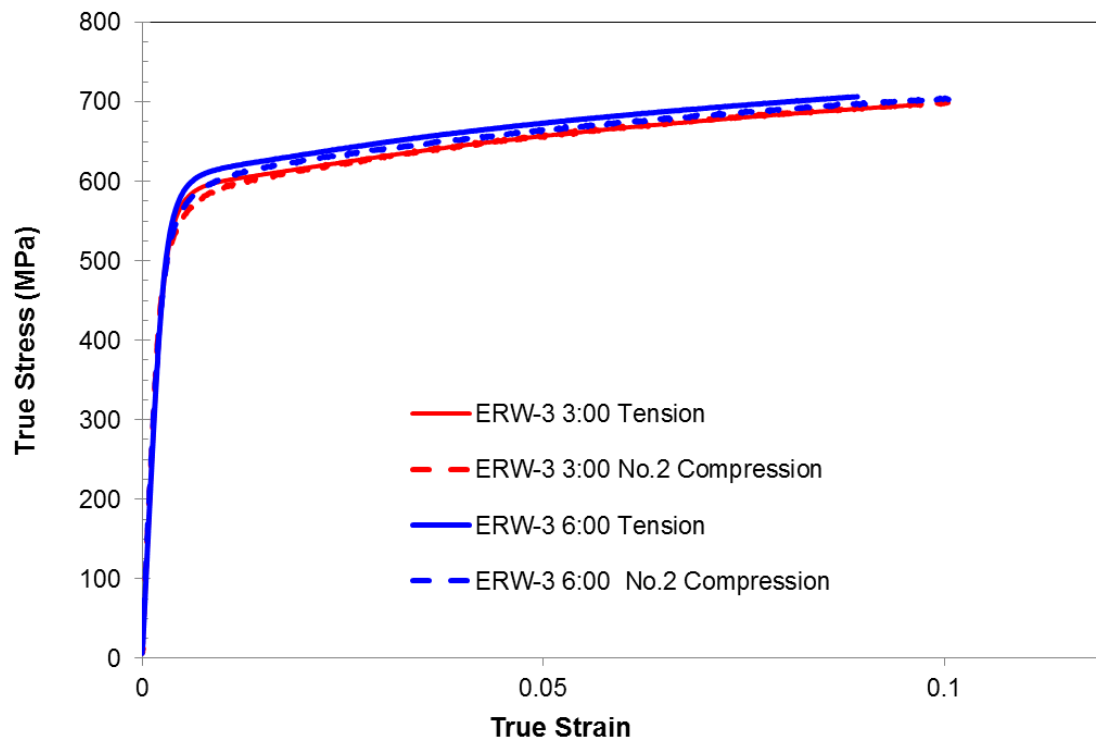


Figure A11 Representative true stress-true strain curves for LPA tension and compression tests for the 3:00 and 6:00 positions of X70 ERW-3 pipe steel

Table A12 LPA Tensile and Compression Yield Strengths for X80-DSAW Pipe Body

Pipe Steel	Orientation – Clock Position	Yield Strength, MPa
X80-DSAW	Tension-3:00	617, 615
	Compression-3:00	615, 605
	Tension-6:00	643, 641
	Compression-6:00	632, 642

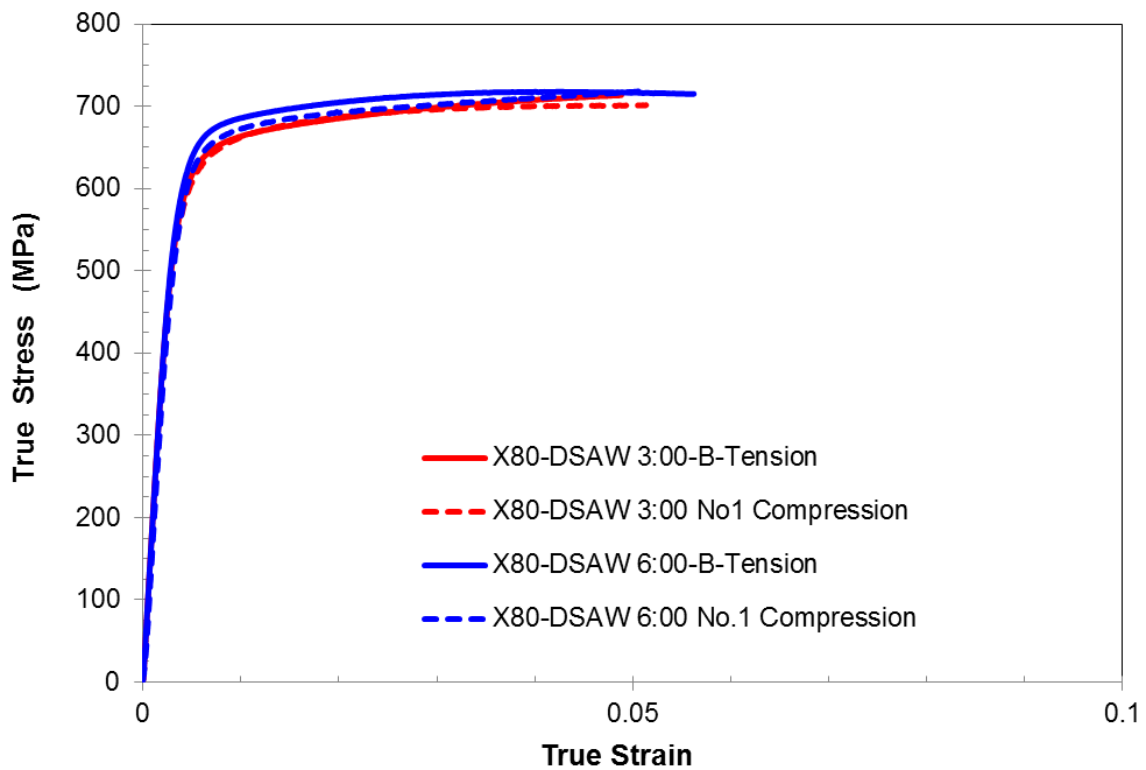


Figure A12 Representative true stress-true strain curves for LPA tension and compression tests for the 3:00 and 6:00 positions of X80-DSAW pipe steel

A.5 Chemical Analysis, Metallography and Microhardness Testing of Selected Pipes

The chemical compositions of the pipe steels were determined by optical emission spectroscopy on sections cut from the pipes used for various full-scale tests in this investigation. The C, S and N were also analyzed by LECO combustion analysis.

A metallographic section was cut across the seam weld of the X65 ERW-1(c) and X80-DSAW pipes. The specimens were mounted in epoxy and prepared using automatic metallographic techniques. The specimens were etched in 2% Nital to reveal microstructural features in the pipe steel base metal and different regions associated with the seam welds. The through-thickness and cross-weld Vickers microhardness traverses were used to further characterize the seam welds, as shown in Figures A13 and A14. The microhardness traverses were completed using a diamond pyramid indenter with a 300-g load with spacing between indents set to ~500 μm .

A.6 Chemical Compositions, Microstructure and Microhardness of Selected Pipes

The pipe steel compositions are listed in Table xx, along with calculated carbon equivalents, which align well with the nominal Grades of the respective pipes. The X65 ERW pipes contained low carbon with ~1% Mn and varying amounts of Ni, Cr, Cu with Nb and different levels of Ti and similar nitrogen. The X70 ERW-3 pipe contained higher Mn, Mo, and Nb along with 0.16% Cu, 0.02 % Ti and similar nitrogen, whereas the X80-DSAW pipe had the higher %C and Mn, and additions of Mo and Cu as well as Nb, Ti with low N.

The microstructure of the X70-ERW-3 pipe steel is shown in the light optical micrographs (LOM) presented in Figure A15. The microstructure consists of a mixed grain structure with very fine polygonal ferrite along with acicular ferrite and possibly bainite. Some irregular (elongated) ferrite regions are also observed and presumably formed from pancaked austenite.

Additional LOM images were taken to characterize different regions within the ERW seam weld. In this case, the microstructures at the mid-thickness of the weld centerline (WMC or bondline (BL)) and three distances away from the BL, i.e., ~750 μm , 3 mm and 6 mm were characterized. The macrograph and micrographs shown in Figures A16(a) and A16(b) reveal that the BL was extremely narrow at the mid-thickness, ranging from about 20 to 50 μm wide. At higher magnification, a very narrow region with a mixture of very fine equiaxed and coarser irregular ferrite grains were observed, as shown in Figure A16(c). The regions immediately adjacent to the BL had coarser irregular ferrite and bainite grains, along with some islands of second phase that are presumably M-A constituents, although this would need to be confirmed.

It is important to mention that the post-weld annealing heat-treatment that is applied to the ERW seam weld results microstructures with varying grain sizes, as can be seen in the series of micrographs in Figures A17 to A19. The images presented in Figure A17 show the microstructure at ~750 μm from the BL is quite similar to that adjacent to the BL, while at 3 mm away the annealed region contained a mixed structure with fine polygonal and irregular ferrite with some bainite along with islands of second phase (presumably M-A constituents). At a further distance of ~6 mm away from the BL, which is close to the extent of the PWHT region partial reaustenization results in a microstructure with fine polygonal ferrite grains and some

original irregular (or elongated) ferrite grains and light and dark etching second phase regions dispersed throughout the structure.

Figure A20 shows the microhardness results obtained for the through-thickness traverse from the OD to ID along the BL (avg. 240 VHN). There was an initial decrease in microhardness from the OD to mid-thickness (254 to 237 VHN) that was followed by a gradual decrease from 243 to 232 VHN moving towards the ID. The cross-weld traverses presented in Figure A21 clearly reveal the differences in hardness profiles for OD, mid-thickness, and ID. The differences in the central region of the seam weld that is consistent with the decreasing hardness results observed for the through-thickness BL. Some softening is also evident at the transition between the PWHT region and the pipe steel base metal (minimum at about ± 8 -10 mm).

Representative micrographs of the X80 pipe steel base metal, presented in Figure A22, revealed a mixed grain structure with a fine polygonal and irregular ferrite along with some bainite and dark etching second phase.

The weld metal (WM) microstructures within the as-deposited columnar regions of the two-pass DSAW seam weld are shown in Figures A23 and A24. The top bead (pass#2) exhibited a columnar structure that contained a high proportion of acicular ferrite within the grain interiors. In contrast, the bottom bead (pass#1) which appeared to have been partially re-austenitized contained very elongated columnar structure with the grain boundaries delineated by equiaxed ferrite grains, while the grain interiors had acicular ferrite along with some dark etching regions and polygonal ferrite grains within the grain interiors. Figure A25 shows the reheated weld metal region that was dominated by fine acicular ferrite.

The microstructure formed in the CGHAZ region (as shown in Figure A26) adjacent to the fusion line of Pass #2, had relative large prior austenite grains that transformed to a mainly upper bainite with the parallel bainitic ferrite laths were separated by elongated discontinuous second phase, presumably M-A constituents. The structure in the vicinity of the Pass#1 was reheated by the deposition of Pass#2, which resulted in some of the previously formed CGHAZ being intercritically reheated, as evidenced by the continuous and/or discontinuous delineation of the coarse prior austenite grains by a dark etching second phase, as evident in Figures A27.

Figures A28 and A29 show the microhardness results obtained for the through-thickness and cross-weld traverses completed for the X80 DSAW seam weld. In the former case, the hardness remains reasonably constant for much of the Pass#2, but decreases noticeable within the reheated region formed in Pass#1 and gradually increases than abruptly decreases at the ID. Cross-weld traverses reveal the variation in microhardness for the three through-thickness positions, i.e., OD, mid-thickness and ID. For the OD traverse, the hardness is reasonable consistent across the as deposited weld metal (nominally 230 VHN) and shows the expected softening through the HAZ. The mid-thickness traverse reveals some higher and lower WM hardnesses and similar softening through the HAZ. In the case of the ID traverse, the influence of reheating which significantly softened the central region of the first pass WM is evident along with much higher hardnesses towards the fusion line/HAZ followed by some degree of softening further away from the fusion line.

Table A13 Chemical Compositions of ERW and DSAW pipe steels

Element wt. %	Pipe Steel Composition			
	X65 ERW-1(c)	X65 ERW-2	X70 ERW-3	X80-DSAW
C	0.058	0.051	0.042	0.062
Mn	1.03	0.95	1.5	1.71
Si	0.18	0.18	0.15	0.1
S	0.008	0.003	0.002	0.004
P	0.007	0.01	0.008	0.004
Ni	0.02	0.1	0.08	0.02
Cr	0.04	0.15	0.08	0.03
Mo	0.003	0.05	0.19	0.18
Cu	0.04	0.23	0.16	0.24
Al	0.031	0.039	0.036	0.022
Nb	0.046	0.029	0.084	0.047
V	0.003	0.003	0.005	0.004
Ti	0.0003	0.02	0.02	0.01
Ca	<0.0010	0.004	0.0039	0.0032
N	0.0073	0.0076	0.0080	0.0031
CE _{IW}	0.24	0.27	0.36	0.42
P _{cm}	0.12	0.13	0.15	0.18
CEN	0.17	0.17	0.22	0.25

$$CE_{IW} = C + Mn/6 + (Cr+Mo+V)/5 + (Ni + Cu)/15$$

$$P_{cm} = C + Si/30 + (Mn+Cu+Cr)/20 + Ni/60 + Mo/15 + V/10 + 5B$$

$$CEN = C + A(C) * (Si/24 + Mn/6 + Cu/15 + Ni/20 + (Cr+Mo+Nb+V)/5 + 5*B)$$

$$\text{where } A(C) = 0.75 + 0.25 \tanh\{(20(C-0.12))\}$$

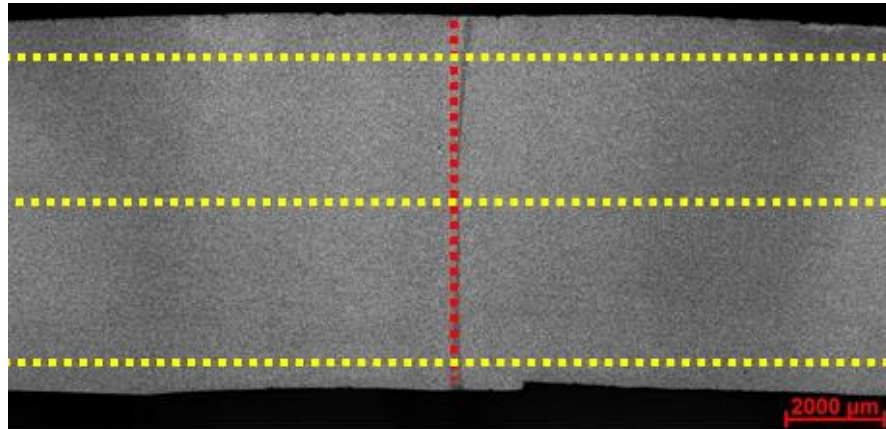


Figure A13 Macrograph showing locations of microhardness surveys along the vertical through-thickness (red dashed line) and cross-weld OD, mid-thickness and ID (yellow dashed lines, respectively) for the X70 ERW-3 pipe.

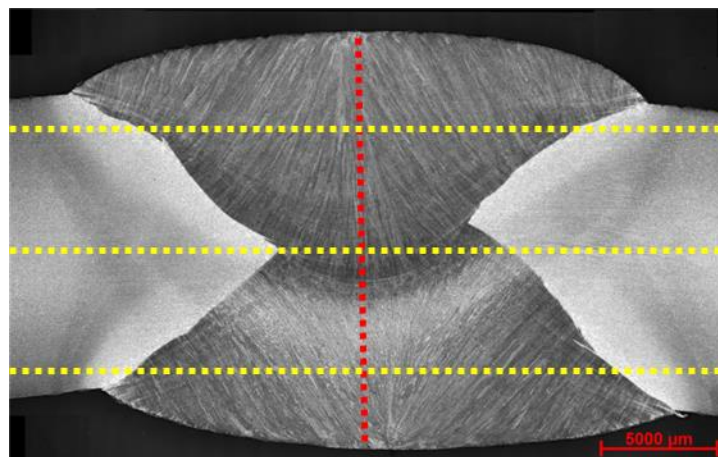
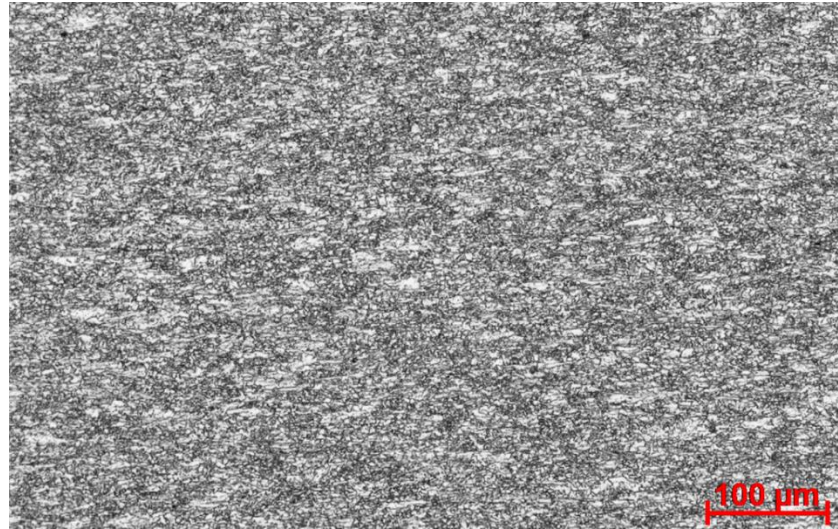
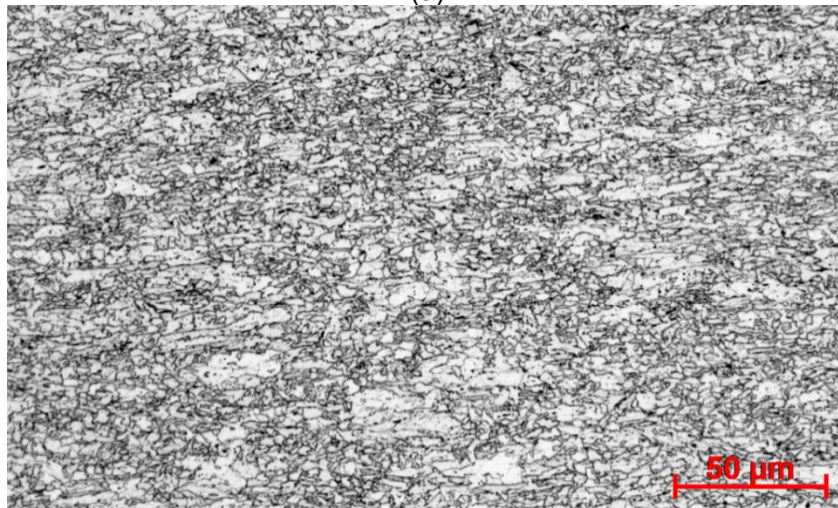


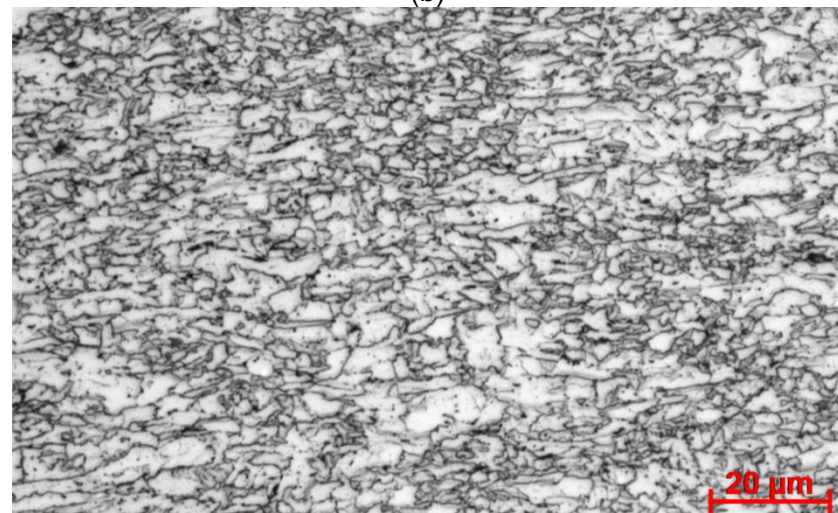
Figure A14 Macrograph showing locations of microhardness surveys along the vertical through-thickness (red dashed line) and cross-weld OD, mid-thickness and ID (yellow dashed lines, respectively) for the X80-DSAW pipe.



(a)



(b)



(c)

Figure A15 Optical micrographs showing microstructure at the mid-thickness of X70 ERW-3 pipe

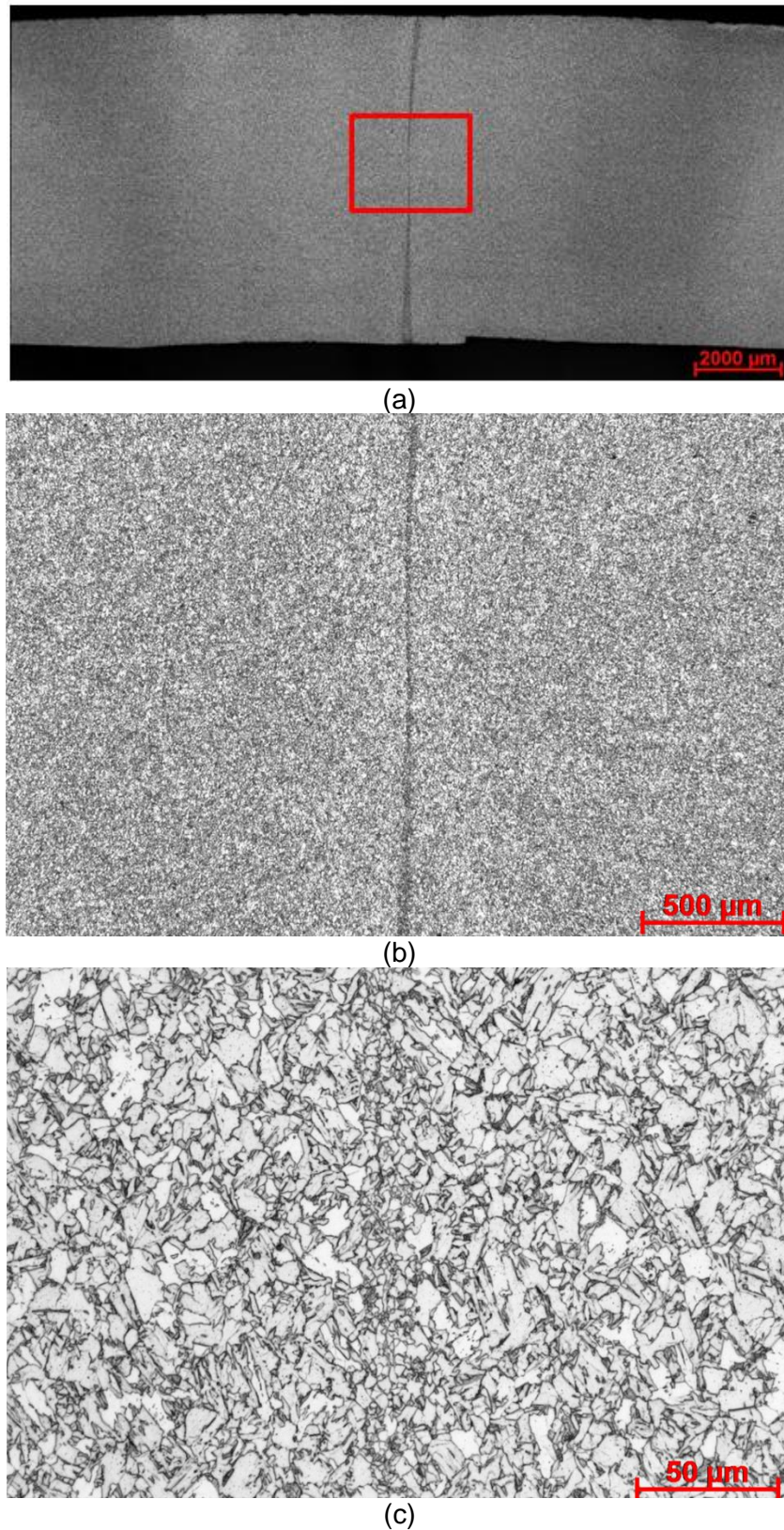


Figure A16 Optical micrographs showing the microstructure at the mid-thickness position along the bondline of the X70 ERW-3 pipe

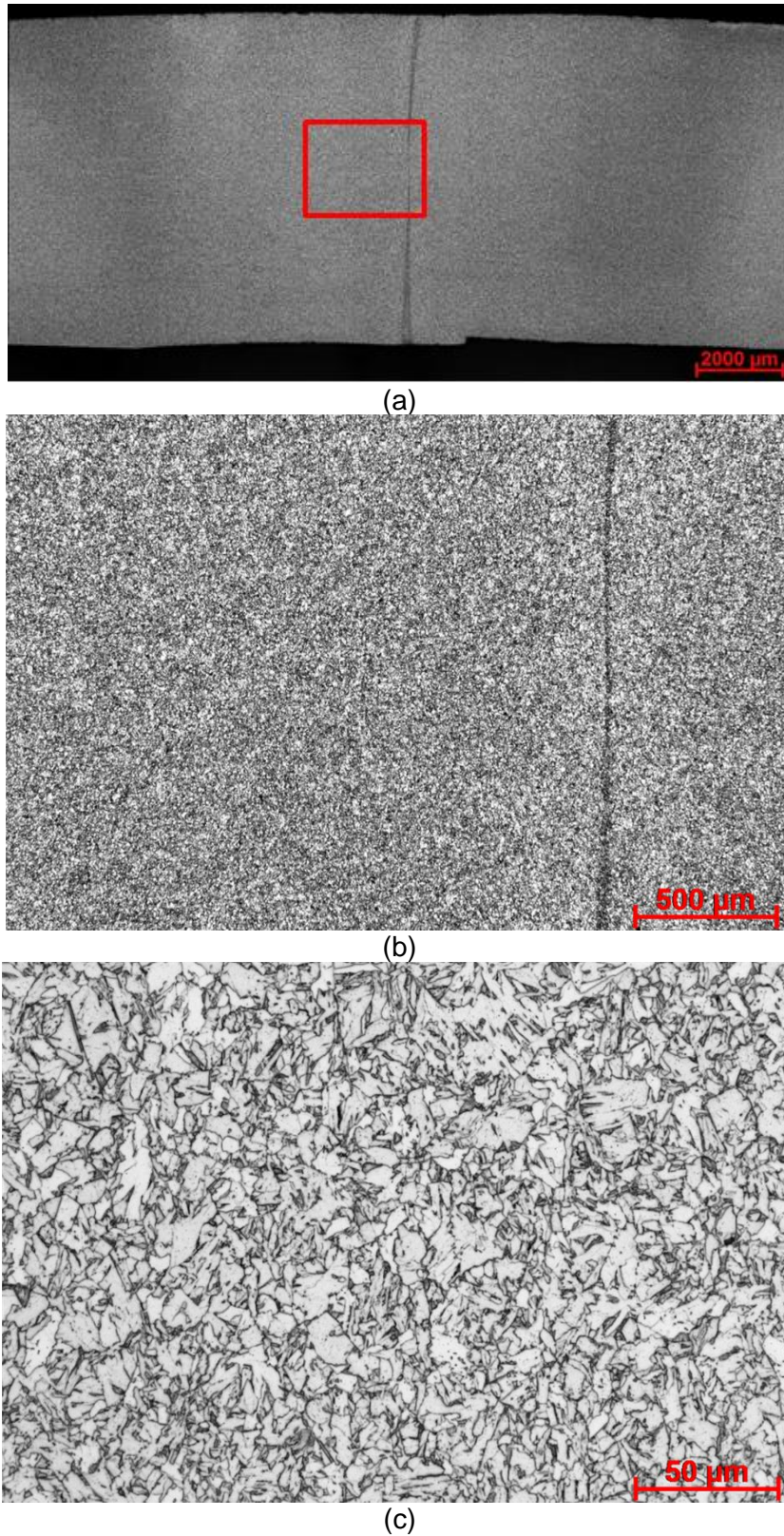
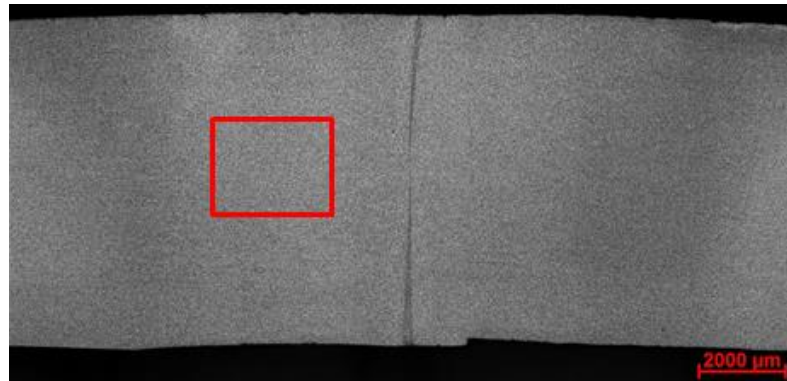
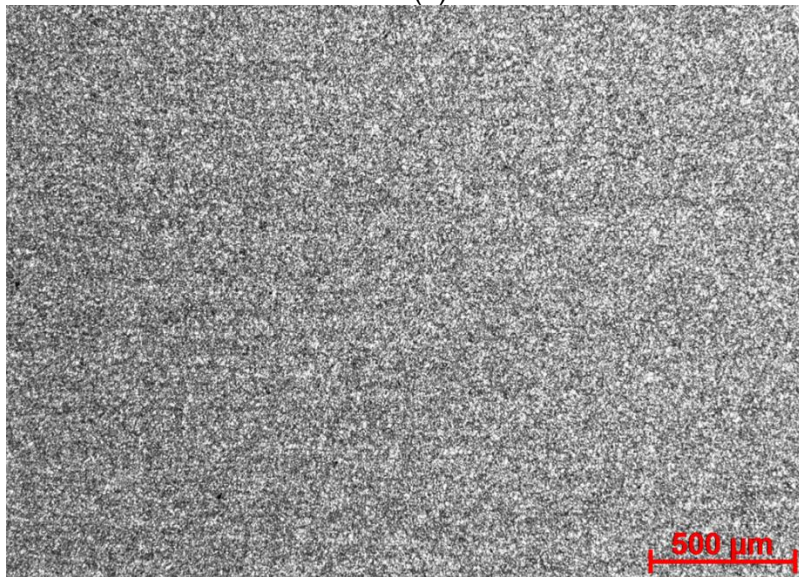


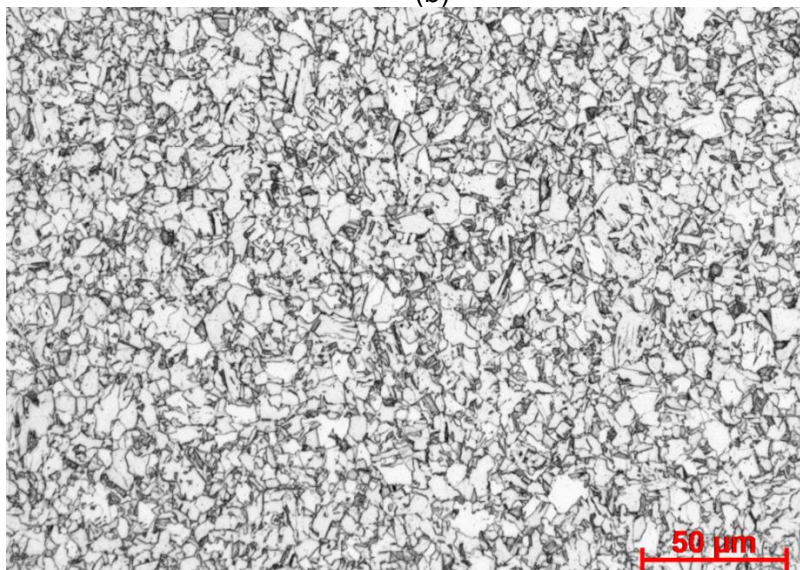
Figure A17 Optical micrographs showing the microstructure at the mid-thickness position $\sim 750 \mu\text{m}$ from the bondline of the X70 ERW-3 pipe



(a)

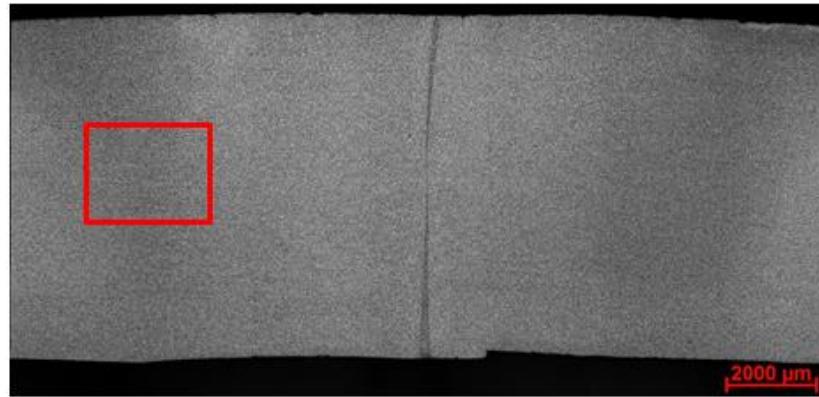


(b)

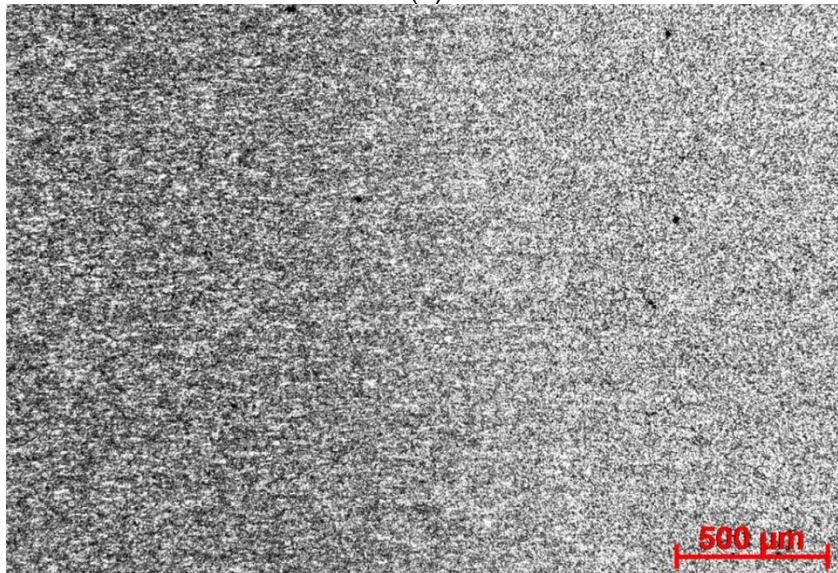


(c)

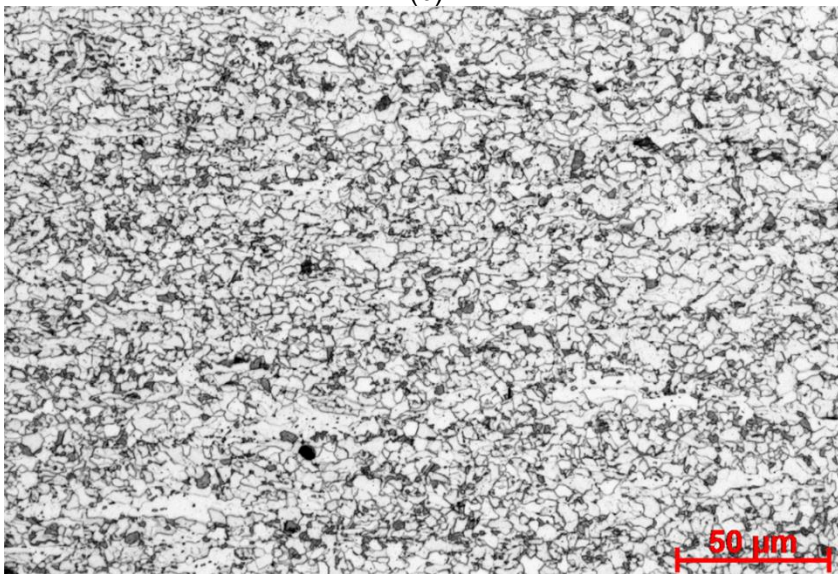
Figure A18 Optical micrographs showing the microstructure at the mid-thickness position ~3 mm from the bondline of the X70 ERW-3 pipe



(a)



(b)



(c)

Figure A19 Optical micrographs showing the microstructure at the mid-thickness position ~6 mm from the bondline of the X70 ERW-3 pipe

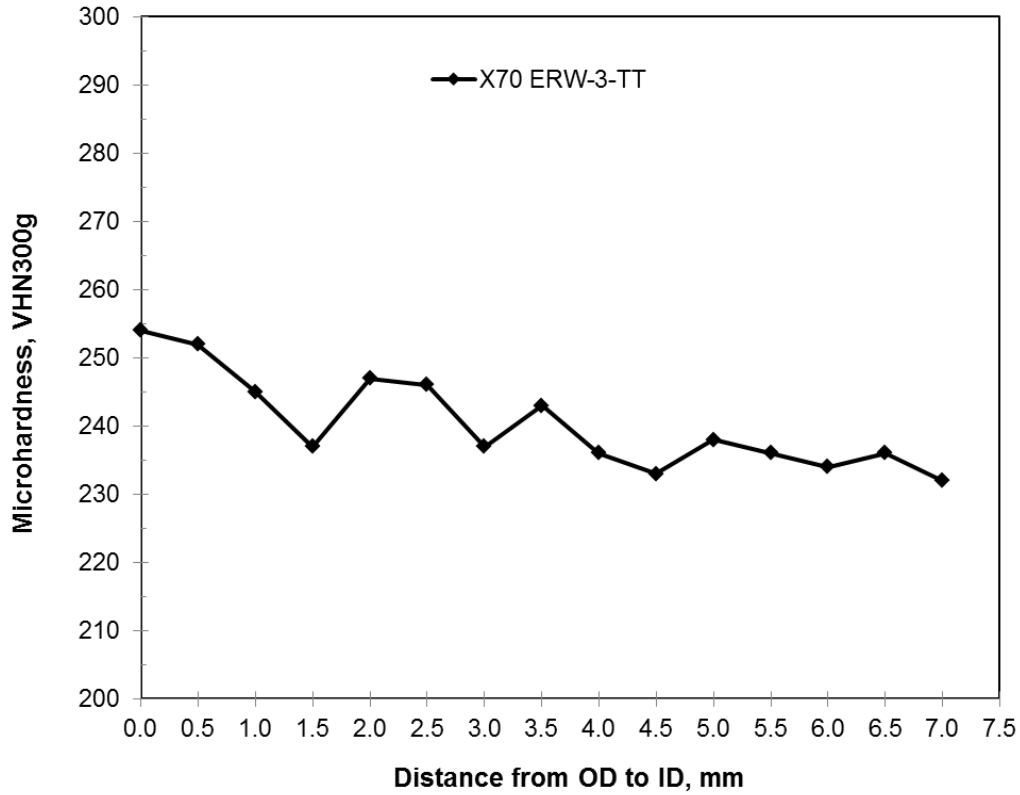


Figure A20 Through-thickness microhardness along the bondline of X70 ERW-3 pipe

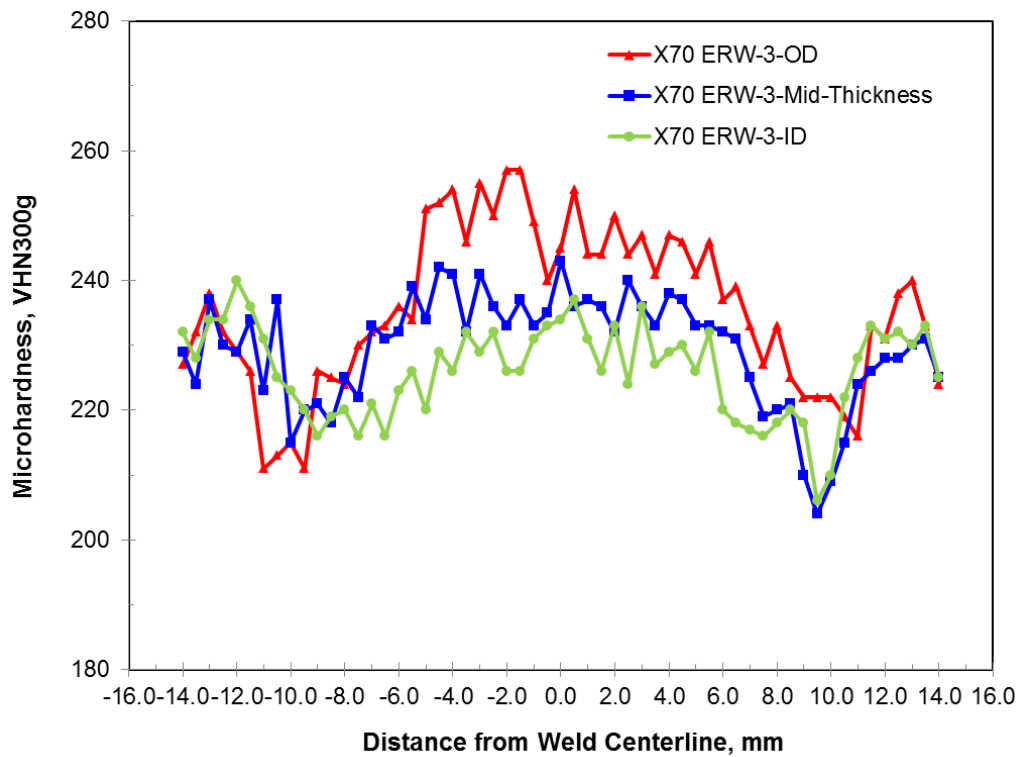
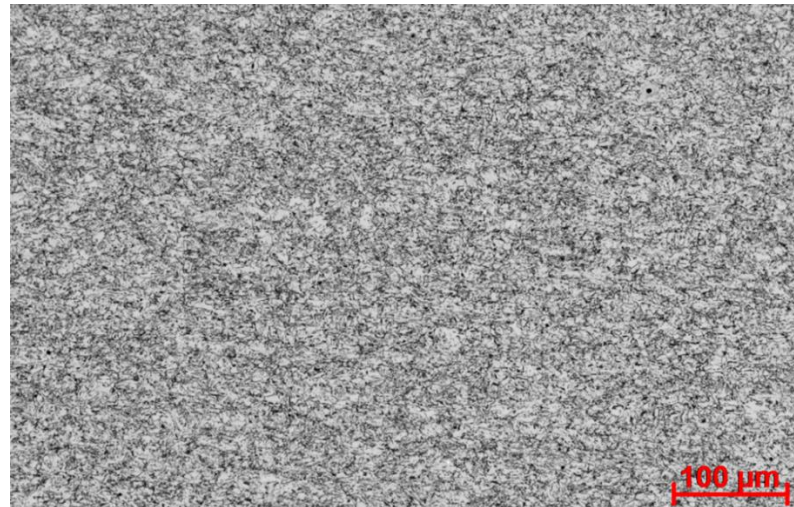
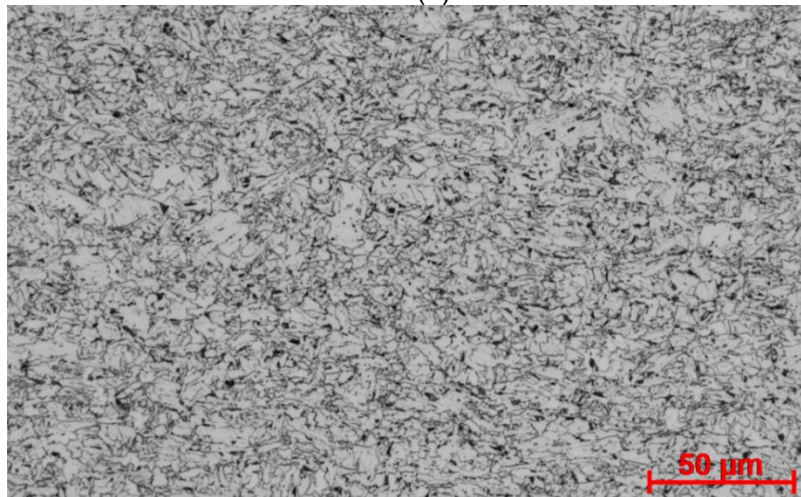


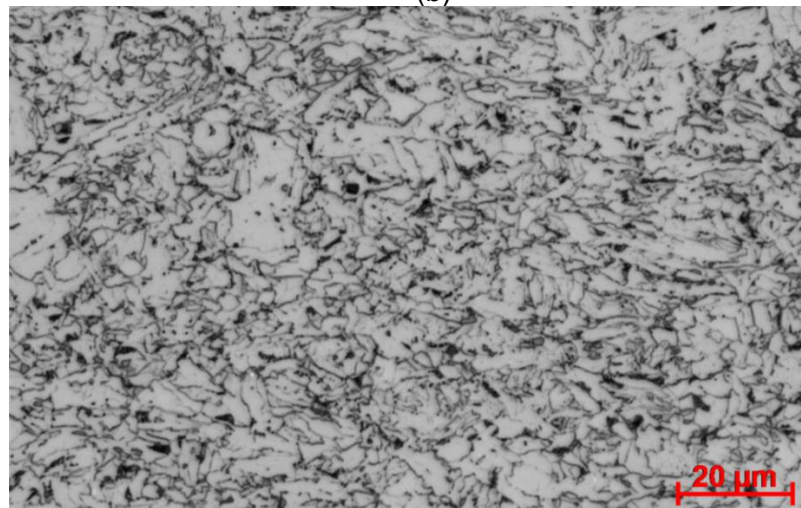
Figure A21 Cross-weld microhardness for OD, Mid-thickness and ID of X70 ERW-3 pipe



(a)

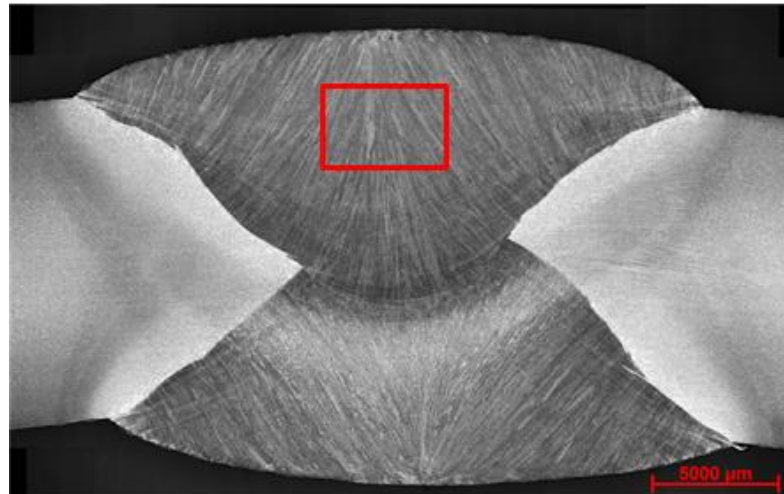


(b)

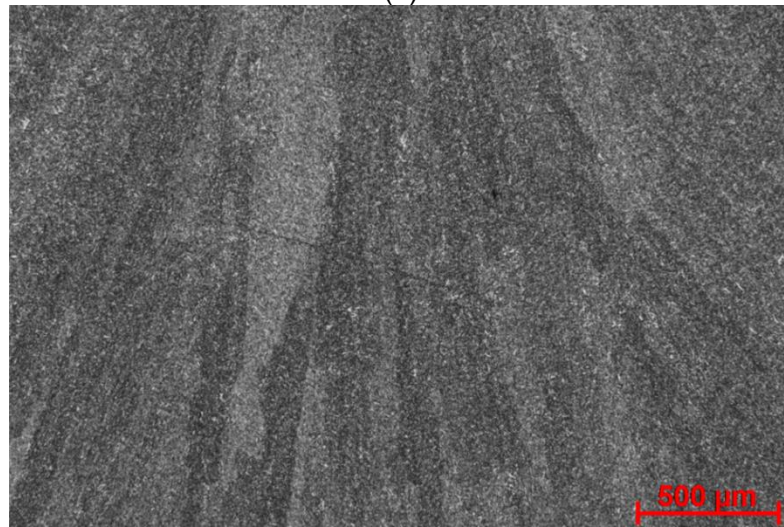


(c)

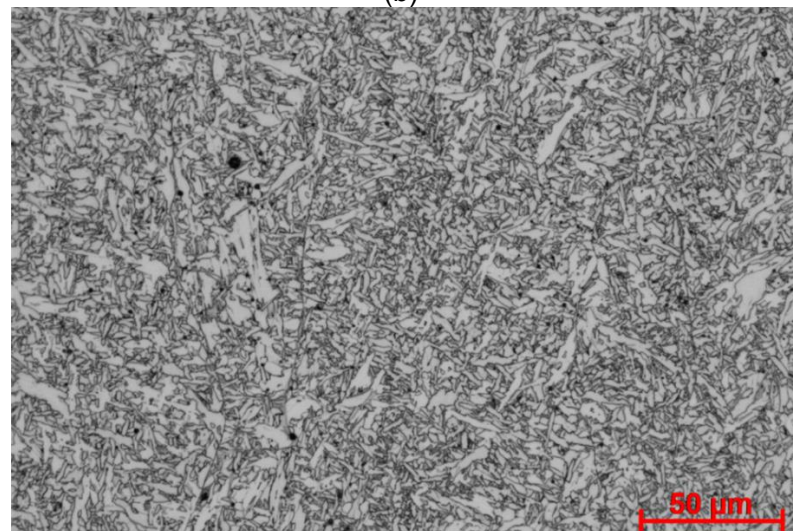
Figure A22 Optical micrographs showing pipe steel microstructure at the mid-thickness for the X80 DSAW pipe



(a)

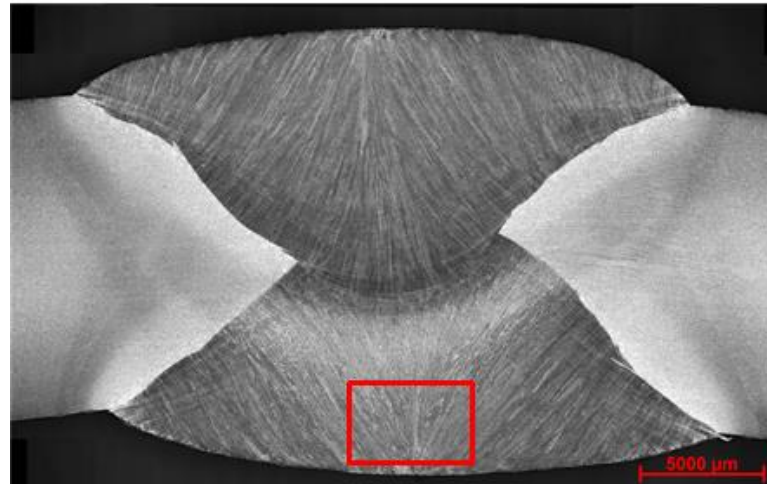


(b)

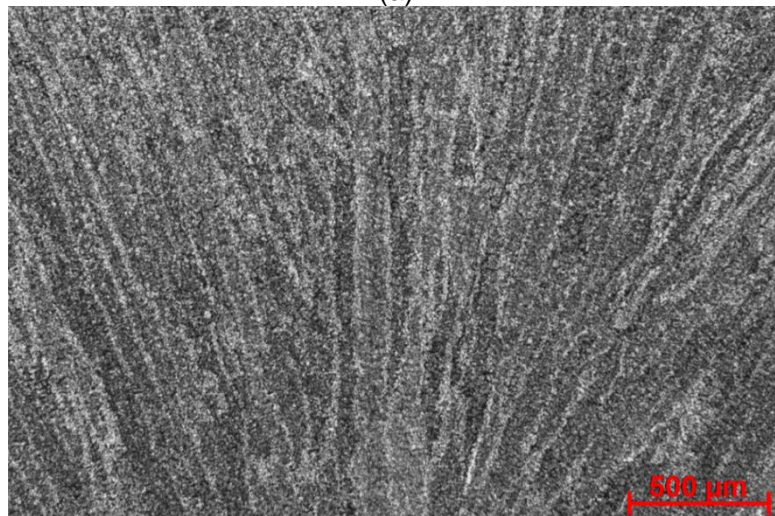


(c)

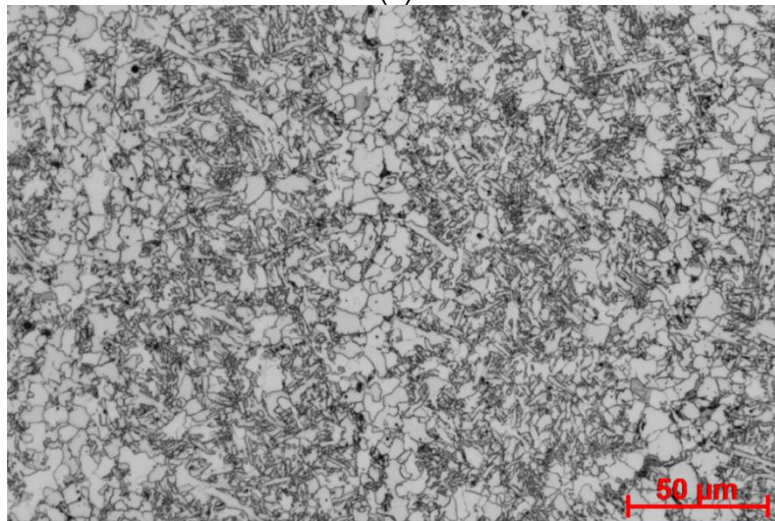
Figure A23 Optical micrographs showing as-deposited weld metal microstructure of OD (Pass 2) for the X80 DSAW pipe



(a)

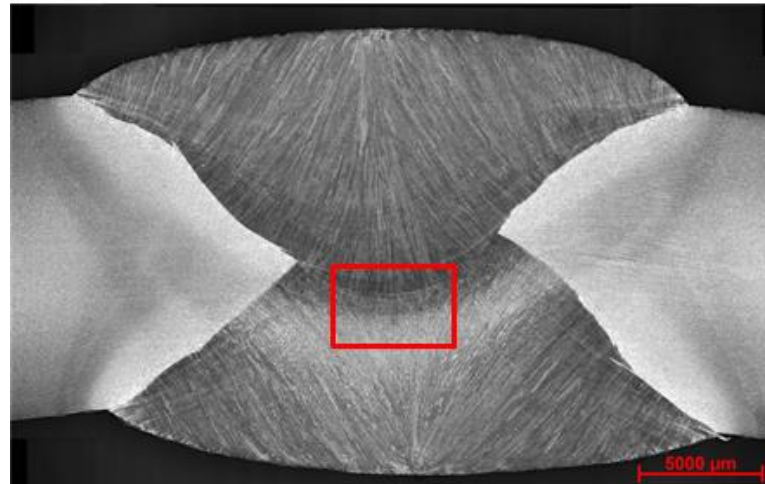


(b)

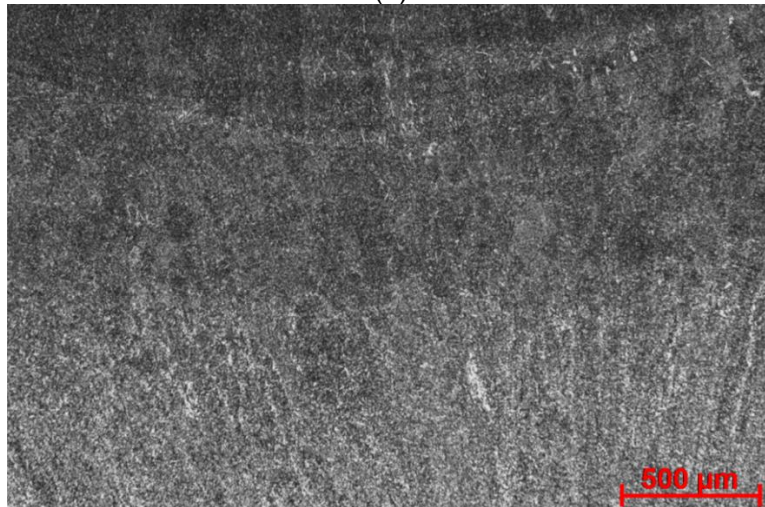


(c)

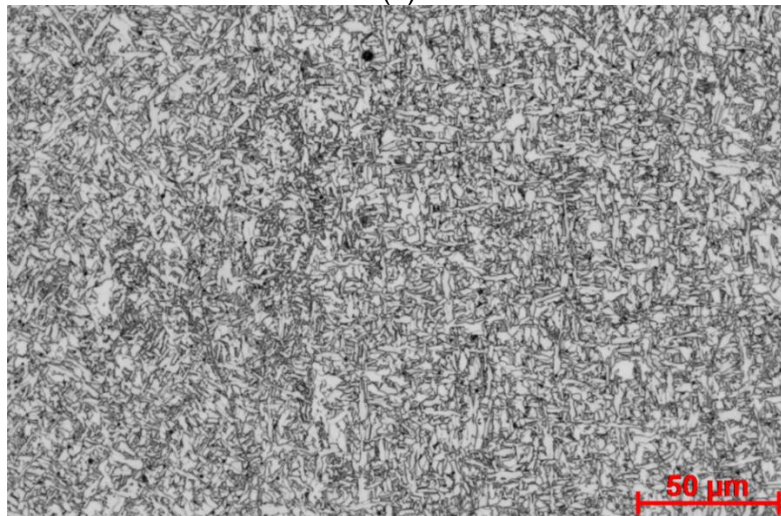
Figure A24 Optical micrographs showing as-deposited weld metal microstructure of the ID (Pass 1) for the X80 DSAW pipe



(a)

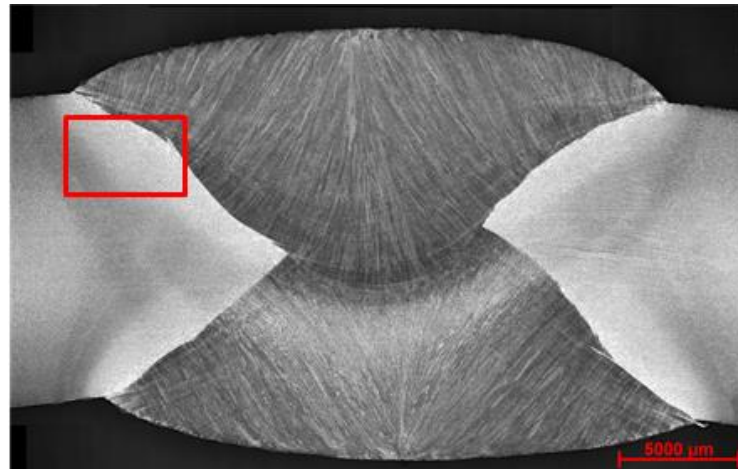


(b)

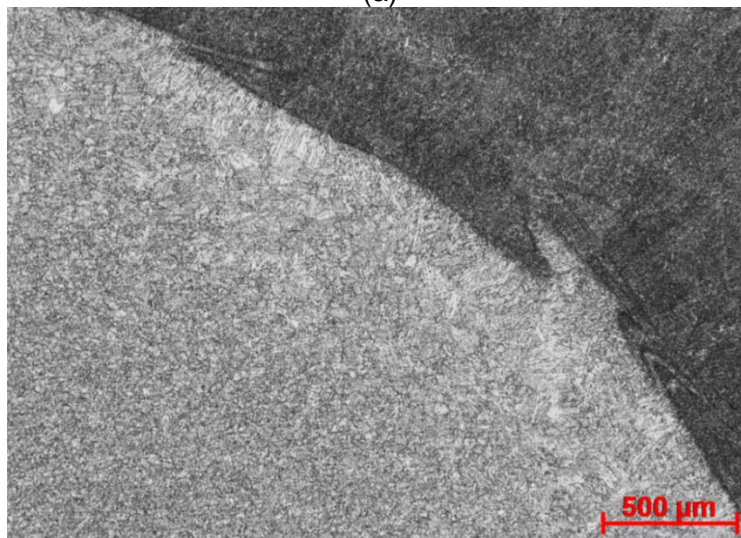


(c)

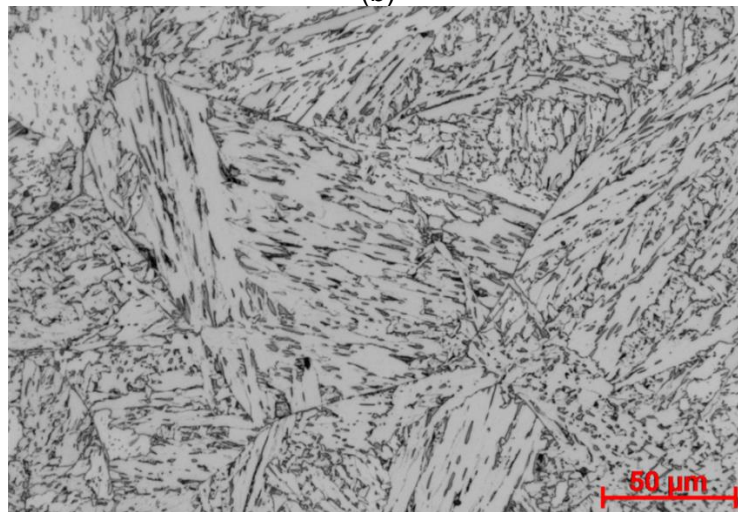
Figure A25 Optical micrographs showing microstructure of the as-deposited region of ID (Pass 1) for the X80 DSAW pipe



(a)

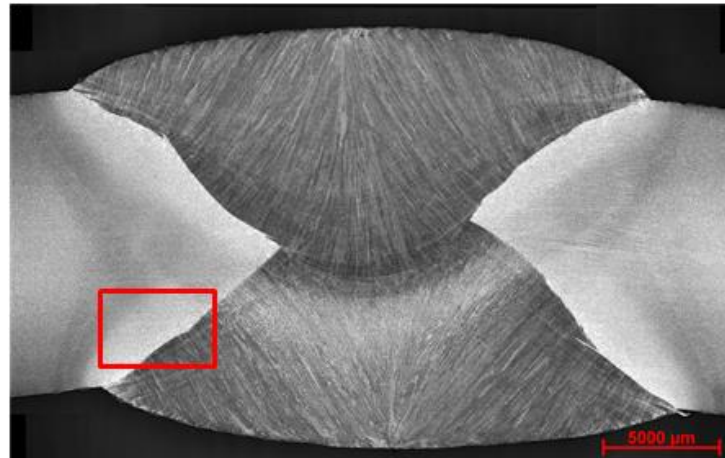


(b)

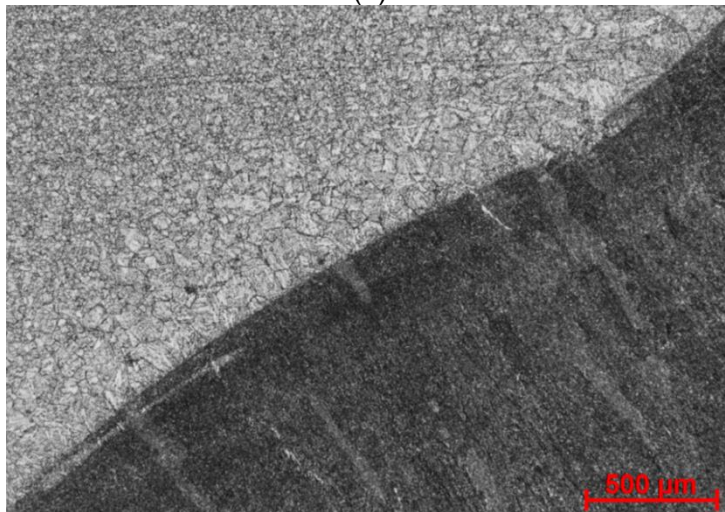


(c)

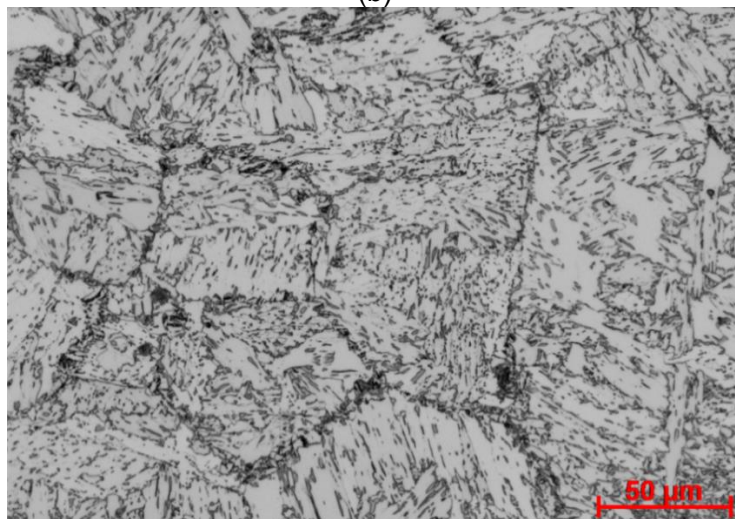
Figure A26 Optical micrographs showing GCHAZ microstructure of the OD (Pass 2) bay region for the X80 DSAW pipe



(a)



(b)



(c)

Figure A27 Optical micrographs showing ICRGHAZ microstructure of ID (Pass 1) region for the X80 DSAW pipe

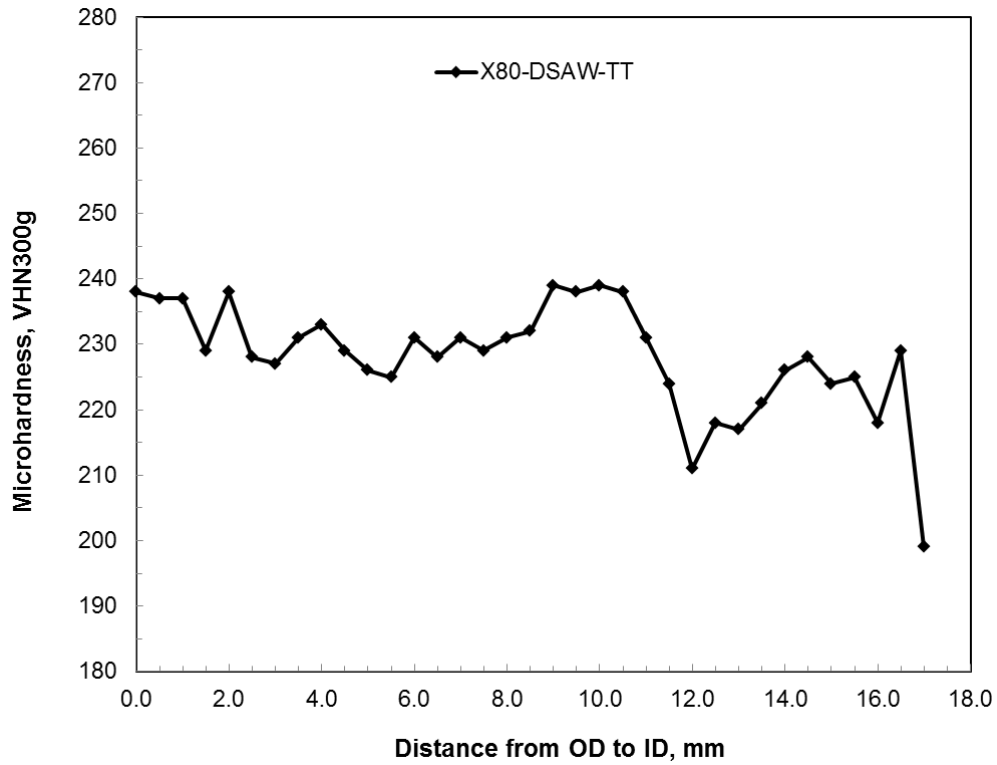


Figure A28 Through-thickness microhardness along the WMC of X80 DSAW pipe

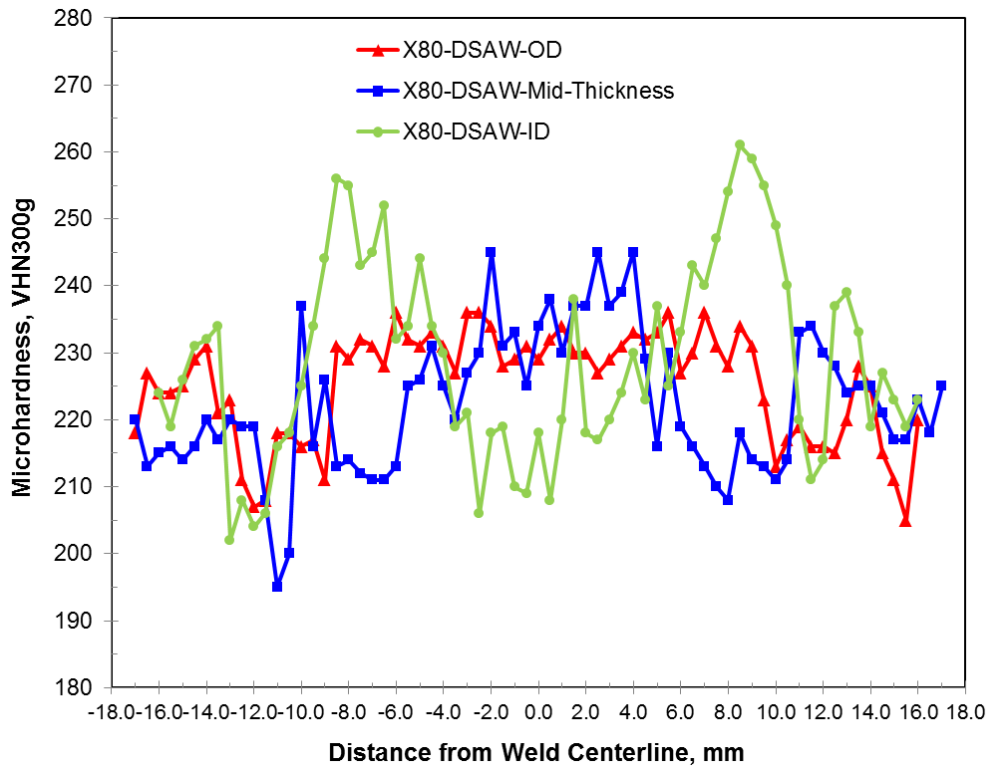


Figure A29 Cross-weld microhardness for the OD, Mid-thickness and ID of X80 DSAW pipe

A.7 References

1. ASTM E8/E8M, “Standard Test Methods for Tension Testing of Metallic Materials”.



Natural Resources
Canada

Ressources naturelles
Canada